The Planetary Science Journal, 6:14 (20pp), 2025 January https://doi.org/10.3847/PSJ/ad9927

The Peregrine Ion Trap Mass Spectrometer (PITMS): Results from a CLPS-delivered Mass Spectrometer

Barbara A. Cohen[1], Simeon J. Barber[2], Aleksandra J. Gawronska[3,4], Feargus A. J. Abernethy[2], Natalie M. Curran[3,4], Phillip A. Driggers[1], William M. Farrell[5,6], David J. Heather[7], Christopher Howe[8], Peter F. Landsberg[2], Veneranda López-Días[9], Andrew D. Morse[2], Thomas Morse[8], Michael J. Poston[10], Parvathy Prem[11], Roland Trautner[7], Orenthal J. Tucker[1], Tristram J. Warren[12], and Stefano Boccelli[1,13]

[1] NASA Goddard Space Flight Center, 8800 Greenbelt Road, Greenbelt, MD 20771, USA; barbara.a.cohen@nasa.gov
[2] School of Physical Sciences, The Open University, Walton Hall, Milton Keynes, Buckinghamshire, MK7 6AA, UK
[3] Center for Research and Exploration in Space Science and Technology, NASA/GSFC, Greenbelt, MD 20771, USA
[4] Department of Physics, Catholic University of America, 200 Hannan Hall, Washington, DC 20064, USA
[5] Space Science Institute, 4765 Walnut Street, Suite B, Boulder, CO 80301, USA
[6] DeepSpace Technologies, 8865 Stanford Boulevard, Suite 183, Columbia, MD 21045, USA
[7] European Space Agency, P. O. Box 299, Noordwijk, South Holland, 2200AG, The Netherlands
[8] STFC RAL Space, Rutherford Appleton Laboratory, Chilton, Didcot, Oxfordshire, OX11 0QX, UK
[9] Luxembourg Institute of Science and Technology, Belvaux, Luxembourg
[10] Southwest Research Institute, San Antonio, TX, USA
[11] Johns Hopkins Applied Physics Laboratory, 11100 Johns Hopkins Road, Laurel, MD 20723, USA
[12] Atmospheric, Oceanic and Planetary Physics, University of Oxford, Oxford, UK
[13] Oak Ridge Associated Universities, Oak Ridge, TN 37830, USA
Received 2024 October 3; revised 2024 November 27; accepted 2024 November 27; published 2025 January 17

Abstract

The Peregrine Ion Trap Mass Spectrometer (PITMS) was a mass spectrometer designed to measure lunar gases. PITMS flew on the first flight of Astrobotic's Peregrine lander via the Commercial Lunar Payload Services (CLPS) program in 2024 January. After launch, the lander suffered a propulsion system anomaly that prevented the mission from reaching the Moon, but PITMS collected 80 high-quality spectra while in cislunar space. PITMS observed abundant outgassing products from the Peregrine lander, including water, MON-25 oxidizer from the propulsion system leak, and traces of combustion products. PITMS data help constrain the nature of the propulsion system failure: oxidizer molecular ratios show that the leak released molecules rapidly enough for them to fully dissociate, and the high observed abundances imply that the oxidizer traveled within the lander surfaces rather than jetting into space. The amount of water offgassed by the spacecraft is substantially more than other planetary spacecraft, so the PITMS results suggest that instruments flying in the CLPS paradigm need to consider lander cleanliness. Though not successful in measuring the native lunar exosphere, the PITMS results showcase the capabilities of a mass spectrometer on board a lunar lander, along with lessons in pragmatism and flexibility that would enable such an instrument to ultimately be successful in the CLPS initiative.

Unified Astronomy Thesaurus concepts: Earth-moon system (436); Mass spectrometry (2094); Ion trapping (2224); Experimental techniques (2078)

1. Introduction

Modern, in situ analyses of the lunar exosphere by mass spectrometry are important to determine the origin, flux, and fate of volatile compounds, linking surface properties and composition to measurements from orbit. The Peregrine Ion Trap Mass Spectrometer (PITMS) was a mass spectrometer experiment on board Astrobotic's Peregrine Mission-1 lunar lander. PITMS was designed to measure the abundance of water at the lunar surface and improve quantification of other exospheric species of interest, such as nitrogen and the noble gases. Ground-level measurements of the type that PITMS was designed for can be combined in space and time with measurements from multiple landing sites and during different seasons to inform models of the volatile flux across the Moon. Thus, PITMS was expected to provide midlatitude data to compare with polar measurements planned by Surface and Exosphere Alterations by Landers (SEAL; M. Benna et al. 2019b), VIPER (J. Schonfeld 2023), the Package for Resource Observation and in-Situ Prospecting for Exploration, Commercial exploitation and Transportation (PROSPECT; R. Trautner et al. 2024), the Lunar Polar Exploration Mission (LUPEX; B. Harvey 2023), and other missions.

PITMS was the result of a successful partnership between NASA Goddard Space Flight Center (GSFC) and The Open University (OU), funded by NASA and the European Space Agency (ESA). PITMS flew on the first flight of Astrobotic's Peregrine lander via the Commercial Lunar Payload Services (CLPS) program. This arrangement was the first of its kind, where NASA negotiated a firm fixed price contract to deliver NASA science payloads to the Moon. Thus, many aspects of the lander hardware and development were not available to the PITMS team, and accordingly, there was no higher-level science "mission" of which PITMS was a part.

The PITMS instrument comprised an ion trap mass spectrometer and a wrapper that mounted it to the lander deck (Figure 1). The mass spectrometer and electronics make up the Exospheric Mass Spectrometer (EMS), built by OU in collaboration with Rutherford Appleton Laboratories Space under contract from ESA. PITMS

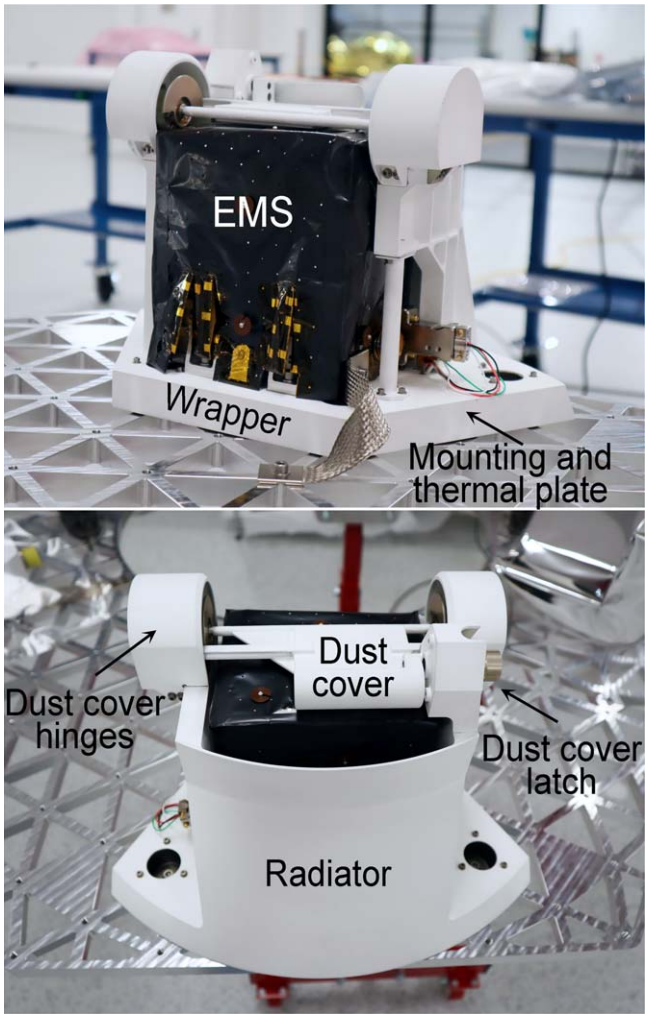

Figure 1. Views of the PITMS instrument mounted to the Peregrine deck. The EMS is shrouded in MLI inside the white-painted wrapper.

sensor development leveraged ESA PROSPECT development to develop a stand-alone mass spectrometer suitable for small lunar landers. The wrapper, built by NASA GSFC, provided structural elements to mate the EMS to the lander, thermal control via a baseplate and radiator, and a deployable aperture cover.

Astrobotic's Peregrine lander flew on board the first certification flight of a United Launch Alliance (ULA) Vulcan Centaur launch vehicle on 2024 January 8. Unfortunately, the Peregrine Mission-1 failed to complete its mission, instead reentering the Earth's atmosphere after 10 days in space. Nevertheless, the lander enabled all the manifested instruments, including PITMS, to operate multiple times and return data throughout the mission. In this paper, we present the mission and instrument details as it was flown and the data collected by PITMS during the mission. All PITMS raw, calibrated, and derived data products, along with a PITMS Data Plan and User's Guide, are archived in NASA's Planetary Data System (PDS; B. A. Cohen & O. J. Tucker 2024) and mirrored in ESA's Planetary Science Archive (PSA).

1.1. Instrument

Details of the PITMS instrument design and development were reported in R. Trautner et al. (2021) and B. A. Cohen et al. (2024); a brief recap is presented here for context. The PITMS ion-optical system comprised a tungsten filament electron source, an ion trap mass analyzer, and an electron multiplier detector. PITMS had a mass resolution of approximately 0.5 amu and was designed to measure species from m/z approximately 10–150. The PITMS sensitivity was determined in this work to be 5.29×10^{-11} mbar per count (Section 3.1).

The EMS consisted of an ion trap mass analyzer mounted above a set of printed circuit boards (PCBs). A 59 × 43 mm aperture at the top of its enclosure, consisting of a rectangular array of 170 holes, each with diameter 3 mm, provided an inlet aperture area of 1202 mm^2 that enabled rapid equilibration with the exosphere external to the instrument. Gases entered the EMS via the zenith-looking aperture and diffused around the mass analyzer cavity. A heated tungsten wire filament emitted electrons to ionize the gases in the cavity. The resulting positively charged ions were trapped in a radio-frequency (RF) field formed by application of suitable potentials to a set of three hyperbolic electrodes. The field could be manipulated to eject the ions onto an electron multiplier detector in order of increasing mass-to-charge ratio (m/z), with detector amplitudes proportional to species abundance. This passive sampling technique was used during Rosetta's flyby of asteroid Lutetia and at 67P during Philae's "bounce" after landing (D. J. Andrews et al. 2012; A. Morse et al. 2015).

The wrapper was made of coated aluminum, providing thermal control for PITMS via a space-facing radiator and survival heaters. The radiator was curved outward to increase surface area and canted at an angle to provide a view to open space after landing. Surfaces that had an external view and the inside surface of the dust cover were painted with white Z93C55 paint, which is slightly hygroscopic. The wrapper also integrated a deployable dust cover to protect the EMS aperture from dust and debris during spacecraft integration, testing, launch, cruise, and landing. The dust cover extended over and around the aperture, providing a tortuous path to prevent lunar dust from entering upon landing.

The PITMS aperture dust cover was not a seal; it was intentionally designed with a small gap to ensure that atmosphere was able to rapidly escape from PITMS as the external pressure decreased at launch and to attempt to measure any species in flight before deploying the dust cover after landing. The gap around the dust cover had an estimated conductance of $\sim 12\,l\,s^{-1}$. This is similar to the effective pumping speed (i.e., pump efficiency combined with system conductance) of a small $80\,l\,s^{-1}$ turbo pump connected to a vacuum chamber via a 3 cm diameter tube ~1 m in length, as is often done for temporary high vacuum chambers in the laboratory. Therefore, PITMS was expected to rapidly evacuate during launch. Once in space, the atmosphere around the spacecraft was expected to significantly lessen; in this regime, the pressure across the dust cover would be expected to equilibrate more slowly with the external atmosphere in the Knudsen regime, where gas molecules would collide more frequently with the instrument and spacecraft than with other gas molecules.

Though the PITMS aperture was covered with a solid plate throughout mission integration and test activities, it was not sealed, and the mission did not include provisions for a dry gas purge at the storage and launch sites. In fact, the lander was exposed to ambient terrestrial atmosphere when in transit from the Astrobotic clean room to test and integration facilities and while in environmental testing. Thus, the expectation was that PITMS would initially outgas significant water brought from Earth before being able to measure the native lunar exosphere.

Figure 2. PITMS mounted to the Peregrine lander Deck D (left) in the Astrobotic clean room and (right) during remove-before-flight activities (with B.A.C. for scale). The Iris rover (N. Potter 2023) is mounted to the underside of Deck D. The PITMS aperture opens to the $+X$ direction of the spacecraft.

The team planned a bakeout of the instrument early in the surface mission for this reason but was not able to bake out the instrument during the actual flight.

PITMS was mounted on Deck D of the Astrobotic Peregrine lander (Figure 2). Deck D was expected to face west in a nominal landing orientation. The Peregrine lander was targeted for the Sinus Viscositatis basaltic lava plain in the northwestern part of the lunar nearside (35.°25N, 319°E). This location was chosen by NASA after PITMS delivery (and therefore after radiator angle optimization for the previous site at Lacus Mortis, 45.°0N, 27.°2E) to create synergies with NASA's future CLPS deliveries, such as the Lunar Vulkan Imaging and Spectroscopy Explorer mission, which will be visiting the nearby Gruithuisen Domes (K. L. Donaldson Hanna et al. 2023).

1.2. Planned Science

PITMS operations were designed to monitor the decay in the lunar exosphere from its postlanding peak, punctuated by any stimuli that create transient increases (for example, lander exhaust desorption, release and operations of rovers, lunar surface desorption and release during the lunar day, and migration from lower latitudes). The nominal operations plan was to commence soon after touchdown (within a few hours) and to continually operate throughout the surface mission. Though the mission ultimately did not land on the Moon, the PITMS team developed science goals and objectives to characterize volatile compounds in the exosphere and released from the surface regolith at the landing site in the context of local geology and lunar-wide processes (B. A. Cohen et al. 2024).

Measurements of exospheric density at the lunar surface are an important complement to measurements at altitude. The Apollo 17 Lunar Atmospheric Composition Experiment (LACE) remains the first and only mass spectrometer to have operated on the lunar surface to date. Critically, while LACE operated successfully for 9 lunar days, the instrument operated mainly during the lunar night, due to high background gas levels that necessitated suspending operations during daytime (J. H. Hoffman 1975; S. A. Stern 1999). In contrast, near-term CLPS landers are anticipated to operate primarily during the lunar day, presenting future instruments with the opportunity to address this temporal gap in measurements of near-surface exospheric composition and density, as well as to measure exospheric variations at a broader range of latitudes. Such measurements would also complement Lunar Atmosphere and Dust Environment Explorer (LADEE) observations from orbit (e.g., M. Benna et al. 2015; A. Colaprete et al. 2016) and build on the LADEE mission's goal of characterizing the lunar atmosphere before perturbation by human activities by characterizing the magnitude and longevity of those perturbations.

1.3. Mission

The Astrobotic team provided multiple public updates during the mission on their website[14] and published a postmission

[14] https://www.astrobotic.com/category/press/

report (Astrobotic 2024); the relevant details are summarized here. After a beautiful launch at 07:18 am UTC on January 8, ULA's Vulcan rocket inserted Peregrine into the planned translunar trajectory without issue, where Peregrine began receiving telemetry via the NASA Deep Space Network. The lander avionics systems, including the primary command and data handling unit, as well as the thermal, propulsion, and power controllers, all powered on and performed as expected. The next event was to initialize the lander propulsion system. The propulsion system was composed of five TALOS-150 667-N thrusters mounted on the bottom of the lander using a hypergolic system of monomethyl hydrazine (MMH) fuel and 25% mixed oxides of nitrogen (MON-25) oxidizer (Astrobotic 2019). The same propulsion manifold was also connected to four sets of three 45-N attitude control thrusters. During initialization of the propulsion system, an anomaly occurred when a valve between the helium pressurant and the oxidizer failed to reseal after actuation (Astrobotic 2024). This led to a rush of high-pressure helium that spiked the pressure in the oxidizer tank beyond its operating limit and ruptured the tank.

The failure within the propulsion system caused a rapid loss of oxidizer that both rendered the propulsion system incapable of accomplishing a landing on the Moon and introduced a difficult-to-characterize dynamic thrust vector to the spacecraft. Though the critical loss of the oxidizer meant that the lander lost the ability to use its descent engine to soft land on the Moon, Astrobotic successfully used the bipropellant system to operate the Attitude Control System (ACS) thrusters nominally, maintaining the spacecraft in a stable, Sun-pointing state.

The loss of propellant and unplanned thrust vector caused the spacecraft to deviate from its intended trajectory and placed Peregrine on a path to intercept the Earth during its planned flyby. Astrobotic positioned the Peregrine spacecraft for a safe, controlled reentry to Earth over a remote area of the South Pacific, which occurred on January 18 at 21:04 UTC, concluding the mission.

During the roughly 10 day operational lifetime, NASA and Astrobotic prioritized maximizing the science and data that the lander could capture in cislunar space. Astrobotic posted regular updates on the time remaining on the spacecraft until the fuel was projected to run out, causing loss of control authority. These expectations were updated each day, because the leak rate was decreasing with time and the spacecraft team better understood how to control the spacecraft. Nevertheless, PITMS and all the instruments operated in emergency response mode each day as if it were the last time.

2. PITMS Operations

The PITMS investigation was conducted by a science team consisting of members from all partner institutions. Peregrine Mission-1 SPICE data begin at 08:09:02 UTC on 2024 January 8, which we take as Mission Elapsed Time (MET) = 0 for all times in this paper. PITMS was able to turn on for the first time approximately 34 hr after the mission start.

PITMS operated in four sessions over the Peregrine mission, for 8.5 hr total instrument operation time. Major successful operations included safely starting up, applying critical software patches, conducting a functional test with filaments and detector off, conducting a functional test with one filament and detector on, acquiring data with the dust cover closed, opening the dust cover, acquiring data with the dust cover open, and downlinking latent data. This allowed the PITMS instrument to collect important information regarding lander offgassing uniquely during off-nominal operations.

As noted, PITMS and all the instruments operated in emergency response mode each day as if it were the last time. Therefore, even though PITMS was able to operate over four sessions, the team could not reasonably create a multisession plan. Additionally, there were data buffer, data rate, power, and operational complexity limitations imposed by Astrobotic on the payloads that, while understandable, made planning PITMS operations challenging. The team prioritized establishing the health and functionality of the instrument, then characterizing performance and environment by taking spectra. The dust cover opening operation, which required powering a different circuit to the instrument, took some time for planning and approval on the spacecraft side and so could not be executed until the third session. The team would have preferred to conduct a bakeout before taking observations, but the power and time needed for this operation was not within scope.

Each time PITMS acquired data, it did so using a scan function (SF) to define the parameters applied to the sensor to acquire a mass spectrum. These parameters drove the ramp rate and amplitude of the radiofrequency (RF) fields and the timing of electron and ion gate operation, which in turn determined data parameters like mass spectral range and resolution. Details of these parameter settings for SFs can be found in B. A. Cohen et al. (2024) and in the PITMS PDS Users Guide. During operation, the PITMS team used science sequences to command the instrument to execute sets of SFs. The SFs were chosen to enable comparison throughout the time PITMS was operational plus several "diagnostic" SFs that would enable the team to better understand instrument performance after the fact.

Table 1 contains the as-run log for PITMS including the experiment number, science sequence and SFs, and the rationale behind choosing the SFs for the experiment. PITMS incremented its Instrument_Timeline_ID (ITL) variable each time it began a new experiment. An experiment may be thought of as a spectrum or group of spectra taken under similar circumstances for a specific science purpose. The first PITMS session assessed the instrument health and functionality by running the instrument with the filaments and detector off (ITL 11). The team planned to subsequently turn the detector and one filament on to collect actual data, but the spacecraft entered safe mode and cut the session short. During the first session, the team discovered that the Astrobotic-allocated onboard buffer and data rate was too low to allow PITMS data packets to be transmitted. The team worked on how to raise the data rate, along with gaining approvals to open the dust cover.

During the second session, we acquired data with the dust cover closed (ITL 12 and 13) and stored the data on the instrument. During the third session, we tested the new data downlink protocols successfully and downlinked latent data, but unfortunately, many of the data were not successfully stored on board the instrument; therefore, we do not have complete spectra for ITL 11 or 12 (described further in the PDS Users Guide). In the third session, experiment 14 was run with the PITMS dust cover still in place over the aperture; then we opened the dust cover and ran ITL 15 (which failed) and ITL 16. Experiments 17 and 18 were run during the last session, after the dust cover had been open for about 1 day. Experiment 18 contains two different science sequences as the team did not have time to send the command to increment the ITL and run a new calibration.

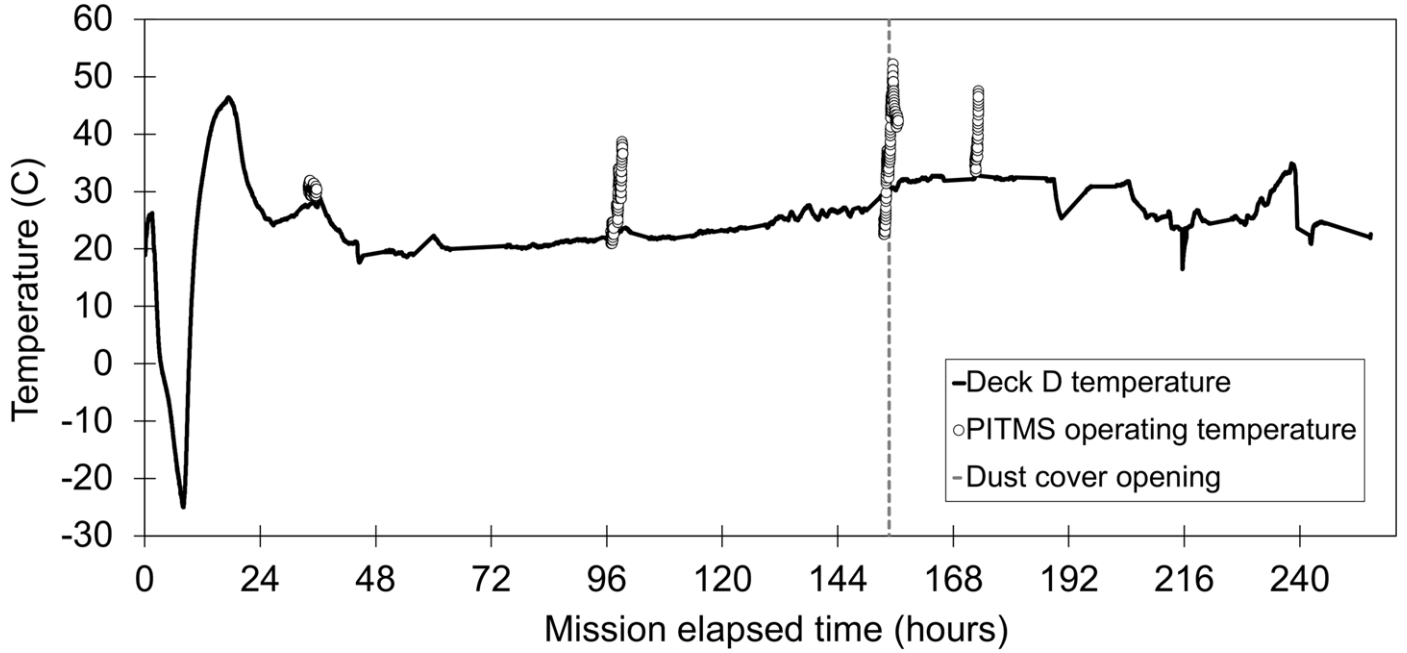

Figure 3. Peregrine Deck D and PITMS operational temperatures throughout the mission. The PITMS ITMS temperature channel (archived in the PDS) is used here as the operating temperature, though the temperature throughout the instrument is not constant (for example, there may be hot spots near the filament). Though PITMS operated in four sessions, only housekeeping data from the first session were used to assess instrument health, and no mass spectra were downlinked.

Table 1
PITMS Experimental Record

Date	Time (UTC)	ITL	Science Sequence	SFs	No. of Cycles	Data Returned	Experiment Intent
2024 Jan 9	16:43						Turn on and software patch
2024 Jan 9	18:09	11	1	1 1 1 1	1	No	Functional test without detector or filament on
2024 Jan 9	19:25						Power removed (spacecraft safe mode)
2024 Jan 12	08:40						Turn on and software patch
2024 Jan 12	09:02	12	2	1 4 1 5	1	No	Functional test with filament and detector on
2024 Jan 12	10:53	13	2	1 4 1 5	4	Yes	SS2 run 4x as a general-purpose scan to compare over time
2024 Jan 12	11:27						Shut down
2024 Jan 14	17:28						Turn on and software patch, data downlink tests
2024 Jan 14	17:59	14	2	1 4 1 5	4	Yes	SS2 run 4x as a general-purpose scan to compare over time
2024 Jan 14	18:28						Deploy dust cover
2024 Jan 14	18:32	15					(Failed) SS2 run 4x as a general-purpose scan to compare over time
2024 Jan 14	19:00	16	2	1 4 1 5	4	Yes	SS2 run 4x as a general-purpose scan to compare over time
2024 Jan 14	19:19	17	11	4 5 11 13	4	Yes	SS11 run 4x to focus on characterizing the lander environment over a wide m/z range
2024 Jan 14	19:49						Science data downlink
2024 Jan 14	20:44						Shut down
2024 Jan 15	12:28						Turn on and software patch
2024 Jan 15	12:41	18					(Failed) SS2 run 4x as a general-purpose scan to compare over time
2024 Jan 15	13:12	18	2	1 4 1 5	2	Yes	SS2 run 2x as a general-purpose scan to compare over time
2024 Jan 15	13:21	18	13	4 3 8 13	1	Yes	SS13 run 1x to include SFs with longer settle time and higher mass resolution
2024 Jan 15	13:28						Shut down

The thermal environment throughout the mission is shown in Figure 3. PITMS was mounted on the top (solar panel side) of the Peregrine Deck D. All the instruments were required to be thermally isolated from the lander deck itself and had their own thermal regulation systems, so temperatures for PITMS were only available during instrument operational periods. A proxy for PITMS temperature during nonoperational periods can be inferred from the Deck D thermocouple, mounted to the top of the deck under the multilayer insulation (MLI). The Deck D temperature history (Figure 4) shows the effect of the propulsion anomaly and subsequent loss of spacecraft attitude control just after launch, where Deck D drifted antisunward and

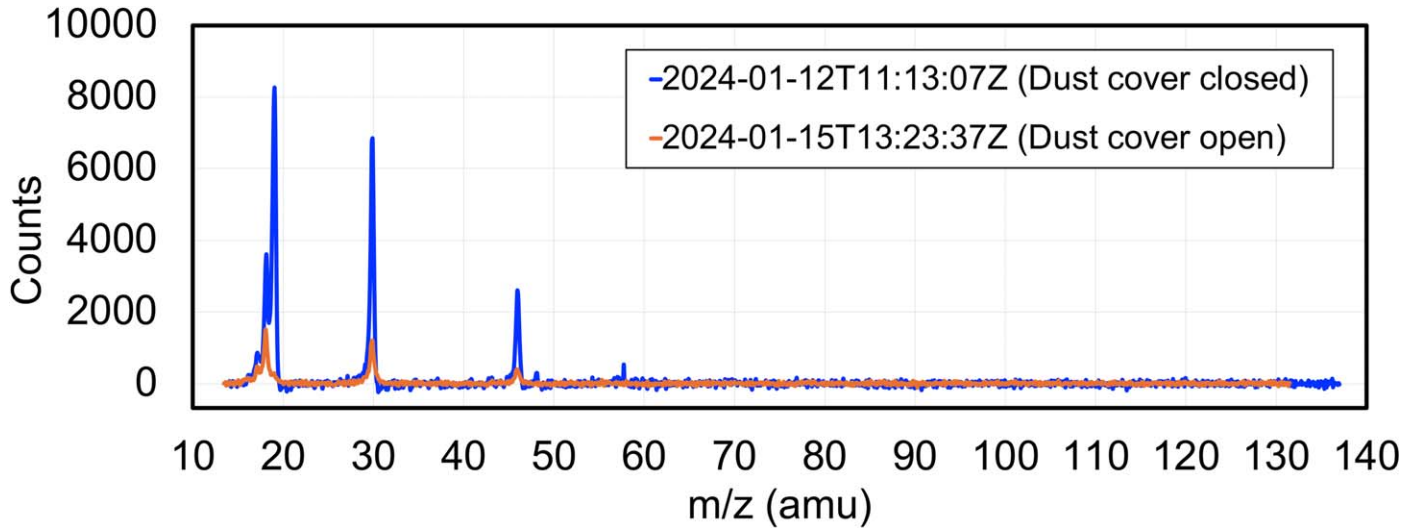

Figure 4. Representative PITMS spectra before and after dust cover opening showing the full range of data and the decrease in both counts and noise when the dust cover was opened.

rapidly cooled. Unfortunately, due to a software safety limit in the lander, the PITMS survival heaters were prohibited from operating. However, as the spacecraft gained three-axis stabilization and pointed sunward, Deck D and PITMS equilibrated to reasonable operating temperatures, and by the time of the first operational period, PITMS turned on and functioned nominally.

During PITMS operations, the interior of the instrument experienced self-heating from the filament. The interior temperatures are shown in Figure 4, where the self-heating over each operational period is visible. The temperature data (included for each spectrum in the archived data) may be used to make further refinements to calibrations described further below and used to infer partial pressure.

3. Results

The science team acquired 84 PITMS spectra. Of these, 77 were complete spectra, three had packet loss, and four were collected with the filament off and therefore were intentionally blank. All data are archived in the NASA PDS (B. A. Cohen & O. J. Tucker 2024) and mirrored in the ESA PSA. The data are accompanied by the PITMS PDS Users Guide, which contains a list of spectra that were acquired.

In general, the quality of the spectra is excellent, with well-defined peaks and low noise, showing that the mass spectrometer worked as expected in space. The spectra acquired prior to the dust cover opening exhibited very high count rates that in some cases reached the limit of the detector system, indicating that the pressure inside the instrument was very high compared with the PITMS design expectations. Both the gas abundance and noise backgrounds decreased rapidly upon opening the dust cover, showing about an order-of-magnitude decrease in all peak areas and decreasing the total peak heights to within the detector's ability to count individual ions (Figure 4).

3.1. Calibration Procedures

We applied a rigorous calibration process, including a multistep m/z adjustment, fitting and subtracting baselines, and conversion to partial pressure using data obtained during the thermal vacuum (TVac) test campaign of PITMS before delivery to Astrobotic. The calibration process is described in detail in the PITMS Data Plan and Users Guide provided in the PDS; this section provides a high-level overview of how raw data are converted to instrument-independent quantities of partial pressure per m/z (mass spectrum).

PITMS generated data by increasing the voltage on the ring electrode to eject trapped species. The specifics of each SF determined the time (and therefore detection bin) of the mass that was ejected. The PITMS processor used onboard measured voltage values to inform an approximate mass calibration of roughly 11.3 bins amu^{-1}. However, as mass spectra were successively collected after the starting onboard calibration, the calibration curve changed due to thermal effects on the electronics, in turn causing mass peaks to drift.

The mass calibration was made in three stages: a linear adjustment appropriate for masses m/z 15–45, a thermal drift adjustment based on known peaks in the linear region, and a nonlinear "bending" adjustment for heavier masses. The linear adjustment was based on TVac data that indicated the mass spectrometer response was linear over the range $m/z = 15$ to $m/z = 45$. The thermal drift adjustment fitted the mass scale to two known peaks within the linear portion of the mass scale, then shifted and stretched the mass scale to force these two peaks to be in their ideal positions along the m/z scale. This correction presupposes knowledge of what species are present and what their ideal mass is. As such, it was applied carefully after preliminary knowledge from the linear mass correction. For the PITMS data set, we chose H_2O^+ ($m/z = 18$) and NO^+ ($m/z = 30$) for this thermal drift correction; details of these species appear later in this paper. Finally, a second-order polynomial derived from TVac data for krypton and xenon was used to correct the high-mass data. The last step shifts the low-mass data by a small amount (0.1–0.2 amu) unique to each spectrum, so the peaks are not always perfectly aligned when comparing spectra with each other.

Because PITMS was not sealed, we could not acquire an instrument-only blank measurement (instrument noise function without any gas), and because of the way the mission anomaly unfolded, PITMS could not acquire a true "background" spectrum. Therefore, we empirically determined and subtracted a baseline from each acquired spectrum to account for

background counts. All baseline fitting and subtraction was performed using OriginPro software,[15] and detailed information and visualization regarding baseline fitting appears in the PITMS PDS User's Guide, but a short summary is presented here for convenience. We smoothed each spectrum using an 11-point averaging window, applied anchor points to the smoothed spectrum avoiding peaks, and then allowed OriginPro to fit the smoothed spectrum using a sixth-order polynomial function, chosen by experience with the PITMS TVac data. We subtracted the fitted baseline function from the raw (unsmoothed) data to produce corrected counts.

We assessed the baseline fit by examining the data variability after baseline subtraction in mass regions without peaks (for example, at $m/z > 56$). Nonpeak counts arise from a combination of electronics noise and ambient molecules and ions hitting the detector. In an acceptable baseline fit, positive and negative noise counts were uncorrelated, and a histogram of the counts could be described by a normal distribution (Gaussian function) centered at zero. We fit the noise data for each spectrum to define the measurement uncertainty and limit of detection (LOD). The 1σ width of the fitted normal distribution was taken as the error in any given data point. The 3σ width of the normal distribution was taken as the LOD, the intensity threshold over which we can identify peaks in individual spectra. In general, the spectra before the dust cover opened had noise levels (LOD) ranging from 144 to 222 counts (182 counts on average across all cover-closed spectra), and after the dust cover opened, the LOD dropped, ranging from 60 to 153 counts (an average of 108 counts across all cover-open spectra). The baseline fits and LOD are released in the PITMS PDS bundle along with the calibrated data.

To convert ion counts detected by PITMS into partial pressure, we developed a quantitative calibration (QC), which defines the relationship between detected ion counts and the volumetric number density of the parent molecule. Because PITMS did not carry a calibration gas system, the QC was developed using PITMS prelaunch TVac test data that contained known calibration gases as well as background gases (e.g., air, water), all measured contemporaneously on PITMS and on the TVac facility Residual Gas Analyzer (RGA) and total pressure gauges. The PITMS QC is based on nitrogen, chosen because N_2 was present throughout the calibration session and produces spectral peaks in the appropriate m/z range. The QC process using nitrogen assumes that the RGA and PITMS were in equilibrium during TVac testing (i.e., encountered the same gases at the same temperatures and the same number densities). The QC additionally assumes that the instrument conditions in the TVac chamber were similar to the instrument conditions during the flight measurements, including instrument temperature, gas molecule temperature, total pressure, and equilibrium conditions. By comparing the partial pressure of the m/z 28 peak measured by the RGA to the total counts attributed to this peak within a 99% confidence interval (see Section 3.3 for more information peak fitting and area calculations), a QC calibration factor of 5.29×10^{-11} mbar per count was adopted for PITMS calibrated data. The uncertainty in the resulting partial pressure is estimated as $\pm 32\%$, derived via a product of (a) error between the recorded partial pressures during TVac testing and the calculated values using the QC factor and (b) systematic errors arising from converting to absolute pressure against the gas-friction manometer. As TVac testing for the QC was primarily completed using SF4, the QC factor may only be appropriate for calibrating data collected using SF4 (see Table 1).

[15] Version 2024; https://www.originlab.com/.

3.2. Data Quality and Artifacts

Observation of the in-flight PITMS data reveals a number of features arising from behavior of the instrument that should be accounted for prior to interpreting the species present in the data.

PITMS peaks encompass about a half an amu on either side of the main species mass, and the peak shape generally follows an asymmetric distribution, with a more gradual ramp-up from the low-mass side and a steeper drop-off in the high-mass side that resembles most closely an asymmetric Lorentzian line shape. This is a characteristic feature of ion traps and results from how ions are trapped and ejected within the ion trap. The instrument RF field forces ions to oscillate in a complex motion according to solutions of the Mathieu equation (R. E. March 1997). Ions of mass m are trapped while the RF voltage is below a critical voltage, $V_c = km$, where k is defined by trap geometry and RF frequency and m is the ion mass. During generation of the mass spectrum, the RF voltage is ramped up to eject ions of successively higher mass. As the RF voltage approaches V_c for a given m, the trapping forces become weaker in the axial z-direction, and ions begin to escape from the trap onto the detector. This results in a gradual increase in ions leaving the ion trap as V_c is approached, until at V_c, the remaining ions quickly (within a few cycles of RF) are ejected into the detector. From that point, there are few remaining ions of mass m; therefore, the high-mass side of the spectral peak drops quickly to baseline.

We used an asymmetric Lorentzian function (LA) to fit the peaks of the form

$$\mathrm{LA}(\alpha,\ \beta) = \begin{cases} [L(x)]^{\alpha} & x \leqslant E \\ [L(x)]^{\beta} & x > E \end{cases}.$$

Increasing the parameters α and β reduces the spread of the tail for the Lorentzian curve $L(x)$, resulting in steeper edges to the line shape. The use of these two parameters enables the spread of the Lorentzian tail to be different on either side of the peak maximum (E). Examination of the data showed that the PITMS response function yielded consistent peak shapes with $\alpha = 1.7$ and $\beta = 4.0$, which were then used in our peak-fitting routine (Section 3.3).

The actual pressure measured by PITMS prior to the dust cover opening was relatively high, well outside the design conditions for PITMS operations. The PITMS electron multiplier works in pulse-counting mode, where one count results from one ion. This assumption holds true as long as ions hit the detector at discrete times and do not overcome the detector dead time. Ground experiments indicate that count limiting (from multiple ions striking the detector within the time constant of the detector) occurs around approximately 11,000 raw counts per data bin. Peaks with raw counts above 11,000 should be treated with caution as they may underrepresent the actual number of ions present in the mass spectrometer. Spectra with peaks exceeding 11,000 raw counts include the m/z 18 and 19 regions in spectra with the dust cover closed and are noted in the PDS documentation and taken into consideration in our interpretations.

Spectra that show these very large signals result in a "dip" in counts following the peak drop-off. These dips below baseline

Table 2
Ghost Peaks Possible in PITMS Data at 0.72 × m/z and 0.87 × m/z of Large Peaks

m/z of Main Peak	m/z of Ghost Peaks
18	13.0, 15.7
19	13.7, 16.5
30	21.6, 26.1
46	33.1, 40.0

arise from known limitations of the electron multiplier detection system when operated at pressures significantly above its designed range. The larger the peak, the larger and wider the subsequent dip. These dips in signal were difficult to accommodate in the baseline fitting and so are generally not accounted for, which may compromise accurate identification of smaller peaks following large peaks.

A known artifact is a small signal produced in bin 1092 during instrument operation. This artifact likely arises from an electronics interaction, although the exact cause of the signal has not been conclusively proven. Though it manifests in the same bin each time and is therefore readily recognized, the bin-to-mass calibration means that it shows up at a slightly different m/z value in each spectrum, generally around mass 51–57.

PITMS operates with a quadrupolar trapping field, but like any such device, the practical considerations in its construction mean that higher-order field components (e.g., hexapole, octupole) are also present, which create regions of reduced stability within the trapping field. Under certain conditions, and particularly at higher operating pressures, a fraction of trapped ions may be ejected from the trap through these field imperfections and thus arrive at the detector earlier than nominal, resulting in peaks at lower apparent m/z. These "ghost peaks" are recognizable because they occur at fixed fractions of the main peak m/z, typically at 0.72 × m/z and 0.87 × m/z. For PITMS spectra, these appear at approximately the masses in Table 2.

3.3. Peak Finding and Fitting and Species Identification

Peak finding and fitting were completed using a custom OriginPro workflow. Peaks were identified in the data using the LOD (defined in Section 3.1) as a threshold and then applying a second derivative algorithm to each spectrum. Each identified peak was fit with an asymmetric Lorentzian line shape (Section 3.2) that determined the peak center and half-width at half-maximum values for each side of the asymmetric peak. We calculated the 3σ width of each side of the peak to determine the bins that encompassed the 99.7% confidence interval. We summed all counts within the m/z limits defined by the 3σ width to arrive at a peak area. When peaks overlapped at the 3σ level, we deconvolved the contribution from each peak by determining the proportion of counts in each bin attributable to a peak based on individual (sometimes overlapping) peak fits, then summing all proportioned counts within the 99% confidence interval of each peak center. This ensured that overlapping peaks were appropriately accounted for using the original data. Once peak areas (in counts) were determined, we applied the QC factor to calculate partial pressures. Because the QC is only applicable to SF4 spectra, we generally focus on SF4 data throughout this work to make quantitative interpretations.

We additionally used peak fitting to investigate whether the instrument temperature during PITMS operation affected species abundance. This behavior might be expected during initial operation, as adsorbed species from launch are driven from the instrument interior. We selected approximately 25 spectra from throughout the mission, spanning time, temperature, and SF. We fit the major peaks that exist throughout the mission at m/z 17, 18, 19, 30, and 46 (see Figure 5). Focusing on these major peaks, we examined their area as a function of the ion trap temperature. The first several spectra have a very clear abundance of water that may be attributed to the first use of the filament and the resulting heating and outgassing effects (see Section 4.2), but after that, no clear trends were observed; most peaks had no change in total area, some trended up, and others trended down. Therefore, we do not further consider corrections from ion trap temperature to abundance of the most prominent species.

Species identification comes from the overall pattern produced in the trap by a given molecule, rather than the m/z of any single peak. Fragmentation patterns arise when some electrons in the source have enough energy to split larger molecules into smaller ones. The fragmentation frequency and type are dependent on the average energy distribution of the electrons emitted by the filament. We used the electron impact fragmentation patterns for candidate species provided by the National Institute of Standards and Technology (NIST) Chemistry WebBook,[16] which were collected at 70 eV. We did not explicitly characterize the fragmentation patterns for each candidate species in the PITMS instrument, which had a nominal incident electron energy around 105 eV, before flight. However, larger electron voltages do not necessarily yield more ions, and eV changes might affect different species differently. We infer from PITMS TVac data for methane[17] (Figure 5) that the PITMS electron source has a "softer" energy distribution than the NIST spectra, meaning that the PITMS spectra have less apparent fragmentation than the NIST spectra. We took this "softer" spectrum qualitatively into account in our species identifications. We also took into account that peaks in the PITMS spectra become very weak at the lower range of the measurable m/z, near the trapping voltage cutoff.

4. Interpretation

Because of the propulsion anomaly and the desire to take measurements while the spacecraft was still operating, the PITMS measurements were made using very off-nominal operations under conditions well outside our design or planning. PITMS was not intended to operate with its dust cover closed (other than to acquire a limited number of spectra as a functional test postlaunch), and the team had planned bakeout operations to clean the instrument's interior prior to making quantitative measurements. Nevertheless, using the spectra PITMS did collect, we can learn about the operation of the instrument, as well as the environment created by the off-nominal spacecraft.

In this paper, we focus our efforts on understanding the broad picture PITMS captured of the spacecraft environment. We use spectra collected using SF4 because SF4 was the only SF for which a QC was developed. In addition, we sum spectra and average data to provide better signal-to-noise ratios (S/Ns),

[16] https://webbook.nist.gov/chemistry/
[17] https://webbook.nist.gov/cgi/cbook.cgi?ID=74-82-8

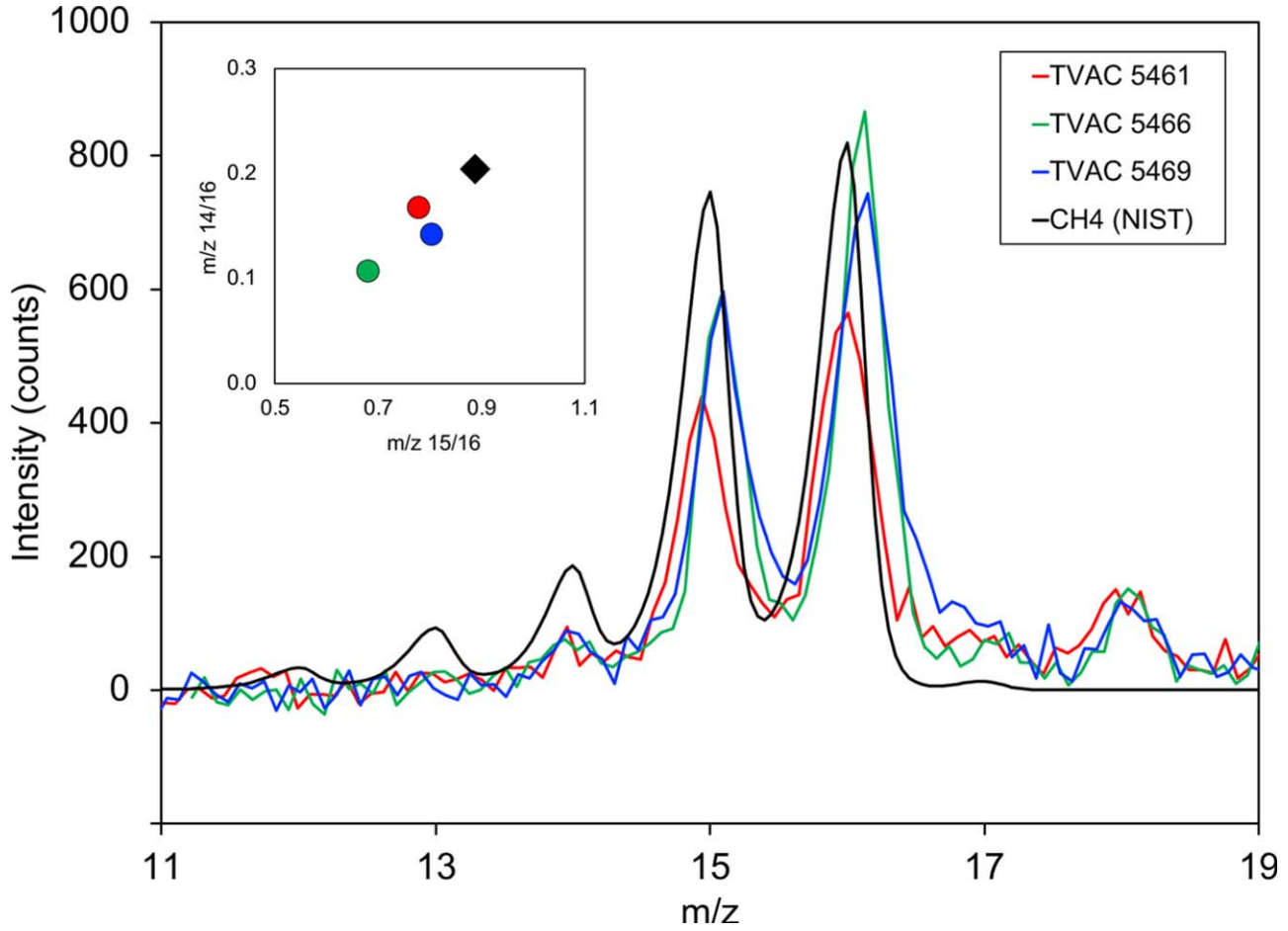

Figure 5. PITMS TVac test data for methane (CH_4) compared with the reference NIST fragmentation pattern. The NIST pattern is convolved to the asymmetric Lorentz function and scaled to the PITMS data for ease of comparison while preserving the relative peak intensity defined by the NIST fragmentation pattern. The inset plots the peak height ratios for m/z 15/16 and 14/16, showing that the PITMS data have lesser abundances of the low-mass fragments ("softer" electron impact energy) than the NIST data.

particularly for small peaks close to the detection limit (Section 3.2) that are otherwise difficult to quantify without significant uncertainty.

4.1. Variation among Spectra

Within each experiment, we collected multiple spectra using multiple SFs. Changes between spectra within each experiment not only depend on the environmental gases being sensed but also include differences in the parameters of acquisition (e.g., trapping voltage, trapping time, ramp rate, and bin width) and changes in the environment of the instrument (e.g., self-heating of the instrument when the filament was on). All the PITMS spectra are available in the PDS for further analysis of spectrum-to-spectrum changes and examination of spectra collected using diagnostic SFs to understand small changes in mass spectrometer behavior.

The exact shape and apparent abundance of each species change slightly in each spectrum (Figure 6), but overall, the changes within each experiment are slight compared with the general trends. When the dust cover was closed, a higher partial pressure was observed within the instrument, manifested as higher counts for all detected species. The higher pressure promotes the conversion of trapped H_2O^+ ions (m/z 18) into H_3O^+ (m/z 19) ions, which can be seen in the 19/18 ratio (described in more detail in Section 4.5). However, as explained in Section 3.2, the m/z 18 and m/z 19 peaks saturated the detector when the dust cover was closed, so care must be taken when interpreting their abundance. After the dust cover was opened, outgassing molecules were able to rapidly escape the compartment, and more "normal" mass spectra were obtained without much variability.

4.2. Total Pressure

As shown in Figure 4, PITMS measured much higher count rates with the dust cover closed than open. As we calibrated the data before and after the dust cover opening event, we found that the pressure in the mass spectrometer (derived below) was much higher than its design limits; in particular, the counts at m/z 18 and 19 exceeded the limits of the ion-counting detector system (Section 3.2) and therefore operated in a regime in which the nominal QC would not apply to these peaks. When the dust cover was opened, the pressure rapidly dropped, and the spectra show that ion counting is effective for all species, including water. In a nominal mission, we would have opened the dust cover on the surface early in the mission and baked out the instrument to estimate and reduce offgassing prior to collecting quantitative science measurements on the lunar surface.

Adding together all counts in a spectrum and then applying our QC factor gives an approximate pressure seen by the

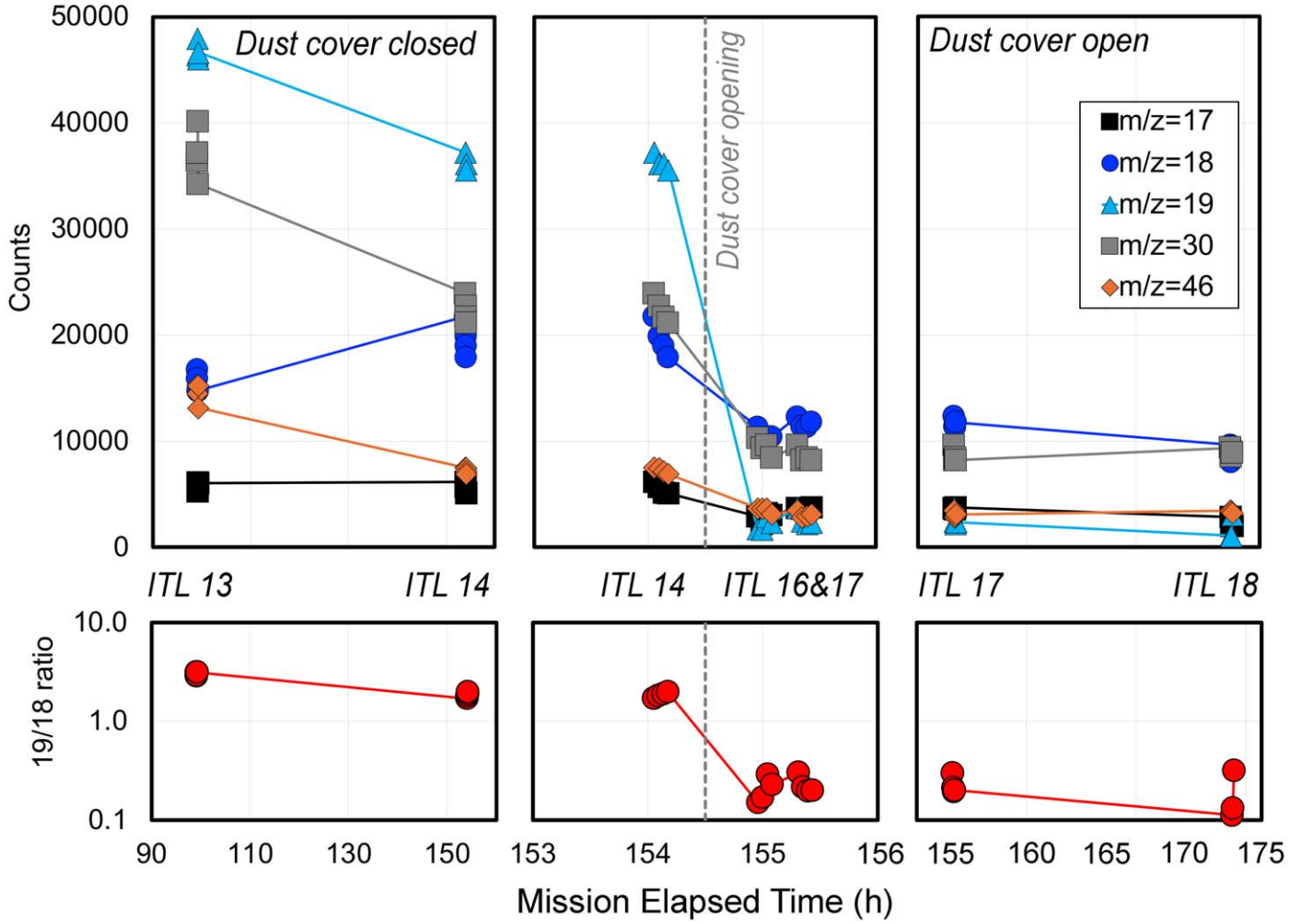

Figure 6. Change in peak area for key regions ($m/z = 18$, 19, 30, and 46) and ratios ($m/z = 18/19$) in SF4 data during the PITMS mission in order of collection (note that the x-axis is scaled differently in each panel to better show data and trends). The small changes or trends within each experiment are primarily the result of changing conditions in the instrument itself, such as offgassing from the filament in the early spectra.

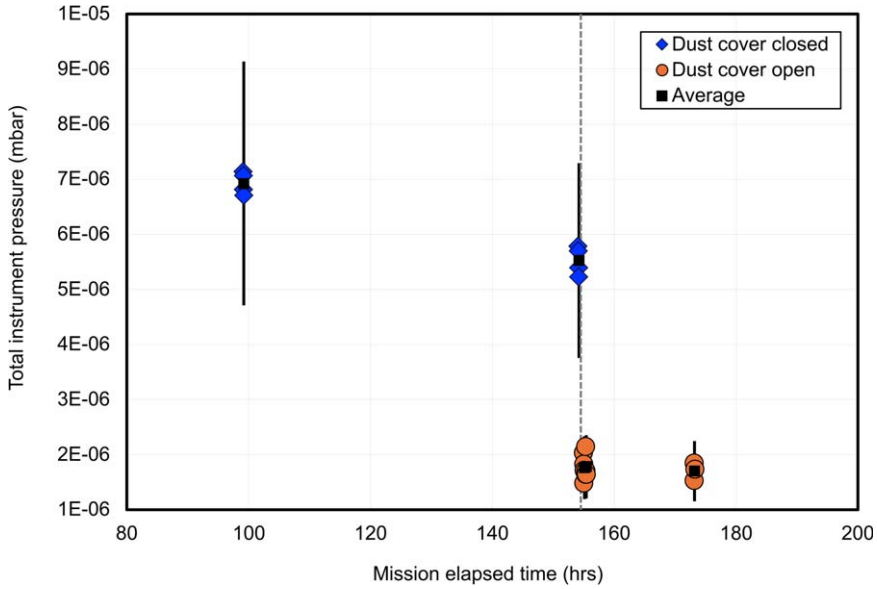

Figure 7. Pressure calculated from the total counts in spectra acquired using SF4 throughout the mission. The gray line shows when the dust cover was opened.

Table 3
PITMS Calculated Total Pressure Using the QC Method

Experiment	MET (hr)	Dust Cover Status	Pressure (10^{-6} mbar)
ITL 13	99.2	Closed	6.92 ± 0.22
ITL 14	154.2	Closed	5.53 ± 0.18
ITL 16	155.1	Open	1.76 ± 0.57
ITL 17	155.4	Open	1.78 ± 0.57
ITL 18	173.2	Open	1.70 ± 0.55

Note. Average and 1σ uncertainty of the data in Figure 7. The calculated pressures prior to opening the dust cover are lower limits, as discussed in the text.

instrument when the dust cover was open and a lower limit on pressure with the dust cover closed. We quantified the total pressure in each SF4 spectrum (nine before the dust cover opened and 11 after opening; Figure 7) and then averaged the results for each time period. The average pressure before opening the dust cover (Table 3) started at $\sim 7 \times 10^{-6}$ mbar and came down a few days later to $\sim 5 \times 10^{-6}$ mbar; however, these are only lower limits because when the dust cover was closed, the pressure so far exceeded PITMS design limits that the instrument was in a count-limited regime (see Section 3.2). After the dust cover was opened, the pressure dropped to $\sim 1.7 \times 10^{-6}$ mbar. The increased conductance through the aperture with the dust cover open enabled rapid equilibration with the external gas density, as evident by the consistent pressure just after opening the dust cover compared with the last data taken 20 hr later. We therefore conclude that at the last time PITMS acquired data, the gas density around the spacecraft was around 1×10^{-6} mbar. These gas densities are extremely high for spacecraft in cislunar space. In the next sections, we quantify the contributing species and use them to corroborate this apparent high pressure.

4.3. Detected Species and Abundance

We quantified the peaks in each SF4 spectrum using OriginPro to search for peaks above the noise threshold as described in Section 3.1. We fit each peak using an asymmetric Lorentzian line shape, deconvolved the peaks using the modeled peak fits, and summed the counts within the peak fit limits. We then calculated the average counts for each peak in every ITL and converted the result to pressure using our QC factor to arrive at an average abundance (Table 4). We then used the team's knowledge of common molecular species that may be present within the terrestrial atmosphere and on board the spacecraft to catalog which species may give rise to the observed peaks. Note that the mass resolution of PITMS was not sufficient to distinguish between nearly isobaric species, so some peaks have multiple possible interpretations. The assignment of particular species to a source will be discussed in the next section.

We interpret the dominant gas inside the instrument as residual terrestrial atmospheric water (H_2O^+ at m/z 18 and H_3O^+ at m/z 19; discussed further below) outgassing from the instrument and the rest of the spacecraft. Strong, persistent features at m/z 30 and 46 are consistent with NO^+ and NO_2^+ from the spacecraft oxidizer, though no peak for $N_2O_4^+$ ($m/z = 92$) was observed (further discussed below). The small feature at mass 48 in the first experiment appears to arise from the $[NO{\bullet}H_2O]^+$ dimer that is thermodynamically encouraged in the trap at high pressures; the analogous $[NO_2{\bullet}H_2O]^+$ dimer is not favored and does not appear. No clear features unambiguously corresponding to nitrogen, oxygen, and/or argon were observed, consistent with full evacuation of the gas phase terrestrial atmosphere.

4.4. Sources

Each PITMS spectrum summed 1000 rapid onboard scans; however, the noise in each individual spectrum precludes searching for minor peaks near the noise level. These minor peaks can be important parts of the fragmentation pattern that enable species to be distinguished from one another to determine sources. Therefore, we used summed spectra from all the experiments before and after dust cover deployment as the best way to look for all present peaks to better identify species. The mass calibration process (Section 3.1) generates a relationship between bin value and m/z values for each individual spectrum and can result in small (0.1–0.2 amu) offsets from each other. For each calibrated spectrum, we used linear interpolation to recast each spectrum onto a common x-axis with m/z intervals at 0.1 amu and summed at each interval. This process has the effect of apparently broadening peaks due to the small mass calibration offsets, but this effect does not negatively affect our overall interpretations.

We used a simple linear mixing model to estimate the source (s) for each species present using a summed spectrum for all data prior to and after opening the dust cover to maximize the S/N. This method does not rely on the quantitative conversion to partial pressure, as it is just looking at the combinations of species (and their fragmentation patterns) that would be expected from each possible source. It does, however, assume equivalent ionization efficiencies for all studied species. The inputs to the mixing model included several individual species and combinations of species. For each species, we used the NIST reference electron impact fragmentation pattern for the relative abundance of each fragment (Table 5) and convolved it with an asymmetric Lorentz function with a 1σ width of 0.7 amu (to account for peak broadening during the summing process) and $p1 = 1.7$, $p2 = 4.0$. We also created linear combinations of these components in molecular proportions appropriate for sources that might be expected in the data, including the terrestrial atmosphere (78% N_2, 21% O_2, 0.9% Ar, and trace H_2, He, Ne, Kr, Xe, CO_2, and CH_4; United States Committee on Extension to the Standard Atmosphere et al. 1976), the spacecraft's MMH fuel ($CH_3N_2H_3$) and MON-25 oxidizer (25% NO + 75% N_2O_4 by weight), and combustion products of MMH and MON-25 (K. H. Lee 2017; L. Hou et al. 2019). Each of these combinations is discussed in more detail in the following sections.

We used OriginPro to iterate a least-squares fit to the summed spectrum, where the amplitude of each component was allowed to vary independently. Because these are summed and not averaged spectra, the absolute peak magnitude and peak center are not meaningful, but the proportion of each component should relate to the abundance of the component in the data. Within the myriad sources of uncertainty in the individual and summed spectra, the best fits to the spectra are shown in Figure 8 and Table 6. The relative abundance of most species is similar with the dust cover closed and open. The major changes are in total abundance (pressure) between the

Table 4
Identified Spectral Peaks, Potential Species, and Their Average Partial Pressure for Each PITMS Experiment

Experiment (ITL)		13	14	16	17	18
MET (hr)		99.2	154.2	155.1	155.5	173.3
Min. *T* (C)		29.8	26.2	36.6	43.9	37.6
Max. *T* (C)		34.5	32.4	43.3	45.9	42.3
Mass (amu)	Possible ion	Partial pressure ($\times 10^{-8}$ mbar)[a]				
16	CH_4^+, NH_2^+, O_2^{++}	5.44 ± 1.21	9.15 ± 1.59	3.02 ± 0.53	3.80 ± 0.61	7.14 ± 1.43
17	**OH^+**, NH_3^+, CH_5^+	30.7 ± 4.97	29.2 ± 4.72	15.0 ± 2.45	19.3 ± 3.11	12.1 ± 2.30
18	**H_2O^+**, NH_4^+	82.2 ± 13.2	104 ± 16.7	55.1 ± 8.83	61.8 ± 9.90	47.8 ± 8.87
19	**H_3O^+**	247 ± 39.6	192 ± 30.7	11.4 ± 1.92	14.2 ± 2.35	9.08 ± 1.95
28	**CO^+**, **N_2^+**, $CHNH^+$	7.49 ± 1.49	13.4 ± 1.19	0.88 ± 0.11	6.08 ± 0.59	—
29	N_2H^+, $CHNH_2^+$	13.2 ± 2.44	11.0 ± 1.62	6.48 ± 1.10	3.23 ± 0.52	2.76 ± 0.56
30	**NO^+**, $N_2H_2^+$, $CH_2NH_2^+$	196 ± 31.4	118 ± 19.0	49.9 ± 8.01	45.5 ± 7.30	47.2 ± 8.74
44	**CO_2^+**, $CH_3N_2H^+$	—	10.2 ± 1.83	5.67 ± 1.01	3.96 ± 0.66	3.07 ± 0.42
45	$CH_3N_2H_2^+$	1.65 ± 0.31	5.15 ± 0.86	0.71 ± 0.09	0.00 ± 0.00	4.12 ± 0.52
46	**NO_2^+**, **$CH_3N_2H_3^+$**	76.9 ± 12.3	38.4 ± 6.18	18.8 ± 3.04	16.3 ± 2.64	17.7 ± 3.29
48	**$[NO{\bullet}H_2O]^+$ dimer** (see text)	6.86 ± 1.24	—	—	—	—

Notes. SF4 data only. Though the mass resolution of PITMS was not sufficient to distinguish between isobaric species, the most likely molecule at the *m/z* is identified in bold. Many of the C, H, and N ions are fragmentation products of MMH as discussed in the text.
[a] Below detection limit denoted by –.

Table 5
Species Used in the PITMS Mixing Models and Their Fragmentation Patterns

Species	Fragment Mass	Relative Abundance	Species	Mass	Relative Abundance
CH_4	12	380	O_2	16	2180
CH_4	13	1069	**O_2**	**32**	**9999**
CH_4	14	2042	Ar	20	1462
CH_4	15	8879	Ar	36	30
CH_4	**16**	**9999**	Ar	38	5
CH_4	17	164	**Ar**	**40**	**9999**
OH	15	90	CO_2	12	871
OH	16	2122	CO_2	16	961
OH	**17**	**9999**	CO_2	22	190
OH	18	50	CO_2	28	981
OH	19	30	CO_2	29	10
H_2O	16	90	**CO_2**	**44**	**9999**
H_2O	17	2122	CO_2	45	120
H_2O	**18**	**9999**	CO_2	46	40
H_2O	20	30	$CH_3N_2H_3$	27	635
H_3O	**19**	**9999**	$CH_3N_2H_3$	28	7262
N_2	14	1379	$CH_3N_2H_3$	29	2151
N_2	**28**	**9999**	$CH_3N_2H_3$	30	1882
N_2	29	74	$CH_3N_2H_3$	31	6321
CO	12	470	$CH_3N_2H_3$	35	5
CO	16	170	$CH_3N_2H_3$	36	43
CO	**28**	**9999**	$CH_3N_2H_3$	38	11
CO	29	120	$CH_3N_2H_3$	39	20
NO	14	751	$CH_3N_2H_3$	40	85
NO	15	240	$CH_3N_2H_3$	41	99
NO	16	150	$CH_3N_2H_3$	42	425
NO	**30**	**9999**	$CH_3N_2H_3$	43	772
NO	31	40	$CH_3N_2H_3$	44	461
NO	32	20	$CH_3N_2H_3$	45	7100
NO_2	14	961	**$CH_3N_2H_3$**	**46**	**9999**
NO_2	16	2232	$CH_3N_2H_3$	47	269
NO_2	**30**	**9999**	$CH_3N_2H_3$	48	8
NO_2	46	3703	**N_2O_4**	**92**	**9999**
NO_2	47	10			

Note. Expressed relative to the most abundant fragment at 9999 (in bold).

dust cover closed and open data and the H_3O^+/H_2O^+ ratio (which varies as a function of total pressure; see next section).

4.5. Water

The most apparent difference in species abundance before and after dust cover deployment is in the H_3O^+/H_2O^+ ratios. All ion trap mass spectrometers have the opportunity for ion–molecule reactions while the trap is actively confining ions that can react with each other and with neutral molecules to produce secondary species; this is considered to be a feature of the ITMS, as it provides additional information not provided by other techniques (R. E. March 1997). The extent to which ion–molecule reactions occur is influenced by two factors: the thermodynamics of the equilibrium reaction in question and the likelihood of collisions occurring. The latter factor is a function of the number density of neutral reactant molecules and the time available for collisions to occur. In PITMS, ions are trapped for relatively long periods of time (up to 6 ms during the ionization and settle phases and then a further 0.1 ms for each amu ramped by the RF before the ion ejection), so ion–molecule reactions can be prevalent, particularly when the number density of neutrals is high.

The spectra obtained with the dust cover closed show clear evidence of the ion–molecule reaction with water: $H_2O^+ + H_2O \leftrightarrow H_3O^+ + OH \cdot \Delta H_r = -102.7\ \mathrm{kJ\ mol^{-1}}$.

The reaction is thermodynamically favorable (the enthalpy of the reaction, ΔH_r, is negative), meaning that it will proceed spontaneously in the left-to-right direction as written. Hence, each time a trapped H_2O^+ ion encounters a neutral H_2O molecule, it is likely to react to produce a H_3O^+ ion (which may also become trapped) and a OH molecule (which will not be trapped, as it is not charged). This will manifest in PITMS spectra as a decrease in m/z 18 (H_2O^+ is depleted by the reaction) and an increase in m/z 19 (H_3O^+ is produced). For scans in which the time available to react is identical, which is the case for at least SF4, SF0, and SF1, the extent to which

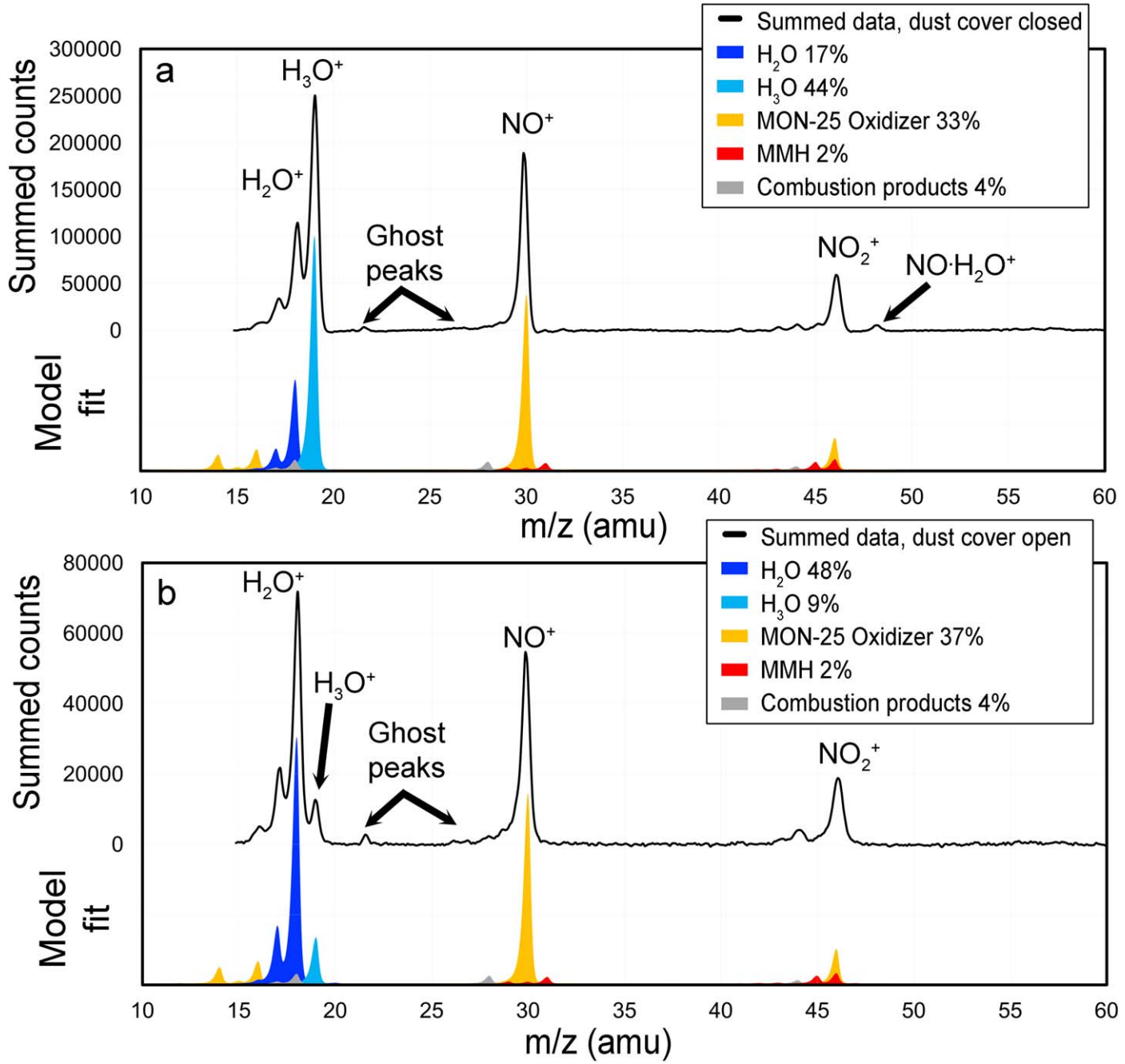

Figure 8. Summed spectra and model fits for all data acquired (a) prior to and (b) after opening the dust cover. The colored curves show the fits to individual peaks and their originating source.

Table 6
Sources of Gases Measured by PITMS Inferred from Mixing Models and Partial Pressure Inferred from the Total Pressure in Table 3

Source	Model Abundance (%)	
	Dust Cover Closed	Dust Cover Open
Water (H_2O + OH + H_3O)	61	57
MON-25 oxidizer (NO + NO_2)	33	37
MMH ($CH_3N_2H_3$)	2	2
Combustion products (H_2O + N_2 + CO + CO_2)	4	4

H_2O^+ is converted to H_3O^+ will be a function of the number density of neutral H_2O in the ion trap chamber.

This phenomenon was exploited to derive an alternative QC for water in PITMS by deriving the partial pressure of water (P_{water}) needed to create the observed H_3O^+/H_2O^+ ratios, particularly for spectra that were count-limited with the dust cover closed. We created this calibration by experimentation on the EMS Ground Reference Model (GRM), a functionally representative model of the EMS within PITMS, housed in a dedicated vacuum chamber at OU. We introduced known amounts of water vapor into the chamber and operated the GRM using SF4 to collect spectra. We then used the PITMS

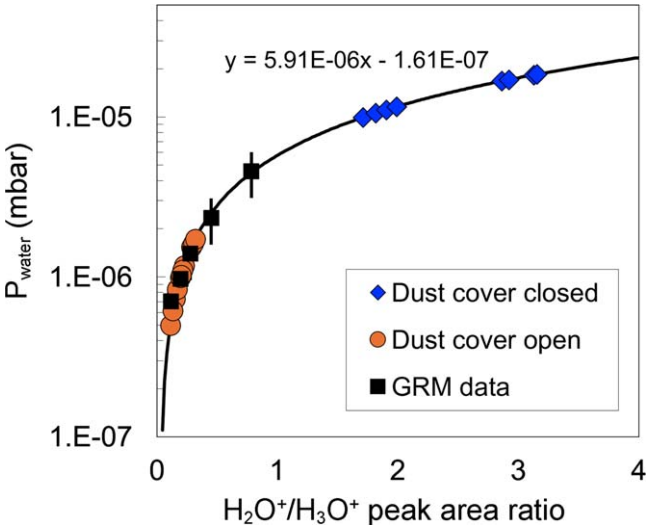

Figure 9. GRM data (black squares) showing the H_3O^+/H_2O^+ peak area ratio as a function of known P_{water} in the test chamber. A linear fit to the GRM data (black line) was used to calculate P_{water} in PITMS data using the H_3O^+/H_2O^+ peak area ratios collected during operation in flight (colored symbols). Error bars correspond to a ±32% uncertainty in the partial pressure measured using the GRM.

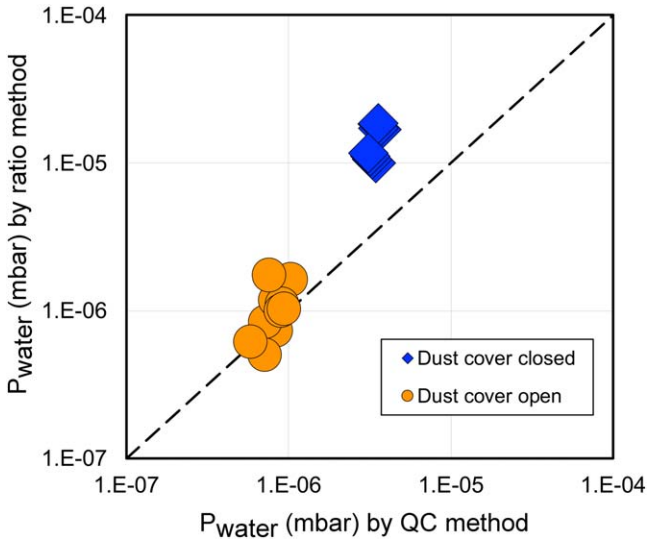

Figure 10. Comparison of two calibration methods applied to PITMS in-flight data for water partial pressure, comparing the GRM-based calibration shown in Figure 9 using H_3O^+/H_2O^+ peak area ratios against the QC (Section 3.2). The dashed line is the 1:1 correlation.

data processing pipeline to process the GRM spectra and derive the H_3O^+/H_2O^+ peak area ratio as a function of water partial pressure within the chamber (Figure 9). This function was adopted to calculate the partial pressure of water from the observed H_3O^+/H_2O^+ peak areas in PITMS flight data, yielding a measure of water partial pressure complementary to that obtained via the QC method. A comparison of water partial pressure obtained via QC versus via the ratio method outlined here is presented in Table 7.

Because the spectra collected with the dust cover closed may be count-limited for the m/z 18 and 19 peaks, both the QC and H_3O^+/H_2O^+ peak area ratio methods provide only a lower limit to the absolute water partial pressure observed with the instrument when the cover was closed. However, the ratio calibration may be a better method for estimating the lower limit of the partial pressure of water in the spectra with the dust cover closed, yielding a higher abundance. In the spectra when the dust cover was open, the difference between the two methods is minimal (Figure 10).

4.6. Oxidizer, Fuel, and Combustion Products

The Peregrine lander propulsion system used a hypergolic blend of oxidizer (MON-25) and fuel (MMH) that spontaneously combusts when the two come into contact with each other. Though Astrobotic did not release details of the magnitude of the oxidizer leak, ACS use, or spacecraft maneuvers, both the oxidizer and fuel and their combustion products are sufficiently well studied (A. C. Wright 1977; K. H. Lee 2017, 2019; L. Hou et al. 2019; H. P. Trinh et al. 2019) that we were able to consider them in our analysis.

We confirmed with Astrobotic that the MON-25 tanks were loaded by adding 25% NO by mass to N_2O_4 under pressure. Using the appropriate molecular masses, this equates to 51% NO and 49% N_2O_4 in terms of number of molecules. However, N_2O_4 would rapidly and completely decompose to $2NO_2$ when released from the high pressure of the spacecraft tank into the extremely low pressure of space (I. A. Leenson 2000; R. Schmehl & J. Steelant 2003). This is consistent with PITMS data, where there is no trace of a feature associated with N_2O_4 at m/z 92 but abundant NO_2 at m/z 46. (Doubly charged N_2O_4 may also contribute to m/z 46, but the lack of observation of other doubly charged ions makes it unlikely that the mass 46 can be solely, or even significantly, ascribed to $N_2O_4^{++}$.)

Table 7
Comparison of the Partial Pressure of Water Observed by PITMS Derived Using the QC Correction Method (Adding Peak Areas for m/z 17+18+19) and the H_3O^+/H_2O^+ Peak Area Ratio Correction Method

	Average P_{water} ($\times 10^6$ mbar)	
ITL	QC Method	H_3O^+/H_2O^+ Peak Area Ratio Method
13	3.60	17.7
14	3.25	10.8
16	0.81	1.07
17	0.95	1.19
18	0.69	0.95

NO_2 itself readily fragments under electron impact to NO^+ (and some O_2^{++} in the harder NIST spectra; Table 5), so the observed peak at m/z 30 arises from a combination of original NO and fragmentation of NO_2. The combined area for peaks at m/z 30 and 46 was used to estimate the pressure of the oxidizer seen by PITMS: between 5×10^{-7} and 9×10^{-7} mbar with the dust cover closed and around 2×10^{-7} mbar with the dust cover open. The exact ratio of NO_2 to NO depends on the fragmentation pattern of NO_2 induced by the actual PITMS electron impact energy, which we established is somewhat "softer" than the NIST spectrum, so our ratios should be considered with a generous uncertainty.

MMH ($CH_3N_2H_3$) has a complex fragmentation pattern that gives rise to multiple small peaks at m/z 41, 43, 45, and 26–27, some of which cannot be readily explained by any other common species (B. B. Brady & J. A. Syage 1995; Table 5). Unfortunately, it is difficult to quantify species at low masses with our PITMS data, so we did not consider any low-mass

Table 8
Combustion Products of MON-25 and MMH

Species	Relative Abundance (%)	
	K. H. Lee (2017)	L. Hou et al. (2019)
H_2	16	0
N_2	31	36
H_2O	33	48
CO	13	0
CO_2	4	16

fragments in our model. Nonetheless, there are enough small peaks at higher-mass, unique m/z locations to interpret them as attributable to PITMS measuring a very small amount of uncombusted fuel (though with a "soft" spectrum where the lower-mass fragments are present in lower abundances than in the reference NIST spectra). Though detections of the small amount of MMH are difficult to confirm in any individual spectrum, these features do appear in the summed spectra for each experiment.

Bipropellant combustion occurred in the Peregrine ACS throughout the entire mission, maintaining spacecraft Sun-pointing stability. Additionally, Astrobotic attempted to initiate combustion in the main engines during the mission multiple times, including at perigee to attempt to raise the orbit and late in the mission to optimize the reentry path. Combustion of MON-25 and MMH (Table 8; K. H. Lee 2017; L. Hou et al. 2019) is a potential source of the small amount of N_2 seen by PITMS, but the corresponding amount of water contributes only a small fraction of the amount PITMS saw.

In the summed spectra across the mission (Figure 8), our mixing models are consistent with ∼4% combustion products that would give rise to trace detections of N_2 and CO_2, along with proportional amounts of H_2O. The abundance of CO_2 at m/z 44 appears to favor the L. Hou et al. (2019) combustion products mix.

Traces of combustion products might be present from other sources that may have been trapped inside the PITMS dust cover, such as combustion from the Centaur upper stage or frangibolts fired at spacecraft separation, but these would be much less likely to appear in data later in the mission. Our tentative detections are consistent with combustion success in the propulsion system as Astrobotic used the ACS nominally throughout the mission. Though the exact times of the main engine combustion attempts were not made public, examination of the PDS-archived SPICE data for the mission show that the only observable velocity changes (after the initial anomaly) occurred during the preparation for reentry, well after the last time PITMS operated.

4.7. Terrestrial Atmosphere

The Astrobotic lander experienced several periods of uncontrolled environmental conditions for transport and test activities and did not undergo a spacecraft-level bakeout prior to flight. PITMS and the Peregrine lander were therefore exposed to the terrestrial atmosphere before flight. We evaluated whether a terrestrial atmospheric signature was observed in PITMS data to understand whether and how much of the observed water could be ascribed to atmospheric gas retained by PITMS.

Of dry atmospheric components, N_2 and O_2 are the most abundant. No O_2^+ was conclusively observed during the mission. A peak at approximately $m/z = 28$ could be interpreted as N_2^+ (Section 4.3), but this peak is minor, ranging from 1×10^{-7} prior to door opening to 6×10^{-8} immediately after door opening and falling to below the detection limit at the end of the mission (Table 4). The N_2 found by PITMS likely originates from sources other than the terrestrial atmosphere, such as the oxidizer leak or combustion. The lack of N_2, O_2, and Ar that could reasonably be attributed to atmospheric contamination is interpreted to result from effective venting of these species after a few days of exposure to strong vacuum and indicates that appreciable amounts of dry terrestrial atmosphere (not including water) would not have reached the lunar surface on PITMS or the spacecraft.

5. Discussion

In this section, we discuss how the PITMS measurements constrain the source and action of the Peregrine oxidizer leak, explore the magnitude of offgassing from the rest of the lander, and consider implications for the measurements PITMS planned to take during the planned surface mission.

5.1. Peregrine Oxidizer Leak

The propulsion system anomaly released a large amount of MON-25 oxidizer that was readily detected by PITMS. Astrobotic did not publicly release where on the spacecraft the oxidizer leak occurred or its intensity or duration; however, it is known from press release images that there was observed damage to the spacecraft MLI on the underside of Deck B, which is interpreted to have been blown out by the leak. PITMS resided on the upper side of Deck D, which is the opposite side of the spacecraft from the inferred leak. The PITMS spectra imply that $\sim 8 \times 10^{-7}$ mbar of oxidizer was present outside PITMS while the dust cover was closed. This is a significant amount that is inferred to be present on the opposite side of the jetting leak.

The rates at which oxidizer must have left the spacecraft under pressure imply that the rapid pressure release resulted in a collisionless regime where the mean free path between molecules increased to meters or longer on trajectories outward from the lander, making it unlikely that jetting oxidizer would be directly measurable by PITMS. When the oxidizer leak appeared, the spacecraft tumbled uncontrollably for about 10 minutes before regaining control authority, then continued to rotate about three axes for about 10 hr until the spacecraft's ACS algorithm was able to account for the thrust provided by the leak and return the spacecraft to a complete Sun-pointing orientation (Astrobotic 2024). This changing spacecraft attitude could have rotated PITMS into a "cloud" of oxidizer, but again, the mean free path of the released oxidizer molecules would not have created an effective temporary atmosphere around the spacecraft. The Peregrine lander remained in a three-axis stabilized position for the remainder of the mission, and examination of SPICE data shows that the PITMS aperture was never in the ram direction of the spacecraft trajectory, precluding molecular entry or concentration by this mechanism (e.g., B. D. Teolis et al. 2015). Additional factors must have occurred for the observed quantities of oxidizer to reach PITMS.

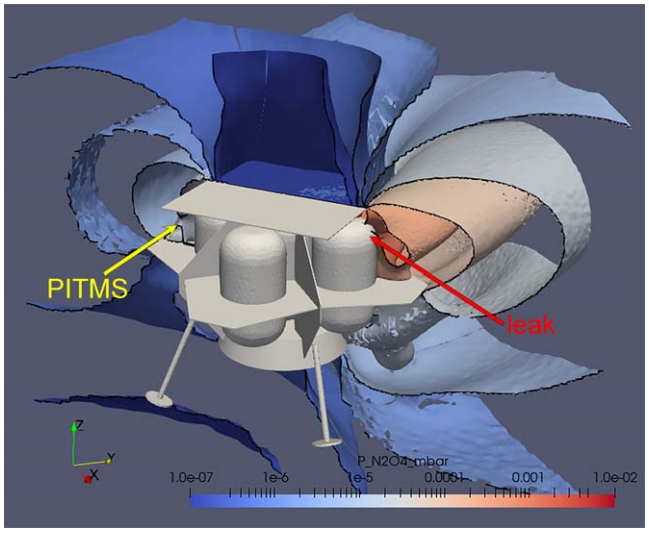

Figure 11. SPARTA collisional simulation of a N_2O_4 leak located on Deck B of the Peregrine lander, localized along a hypothetical MLI seam line. The color bar shows the pressure of N_2O_4. This simulation is done with an open geometry and shows that a considerable amount of gas flows through the spacecraft, enabling it to reach PITMS on the other side of the lander.

One likely scenario might be if the oxidizer leak, which we know displaced MLI, sent oxidizer along paths inside the MLI and spacecraft in addition to being jetted out. We ran collisional direct simulation Monte Carlo simulations using SPARTA[18] of a MON-25 leak localized along a hypothetical seam line. Figure 11 shows the pressure of MON-25 in mbar for a leak flow rate of 10^{22} molecules s^{-1} in a single-species simulation. Qualitatively, the shape of the contours would be similar if a larger or smaller leak were simulated, though the absolute values would be larger or smaller. This simulation was done with an open geometry (based on a simplified CAD model) that allowed a considerable amount of gas to flow through the spacecraft. If the leak were on Deck B, molecules could reach PITMS on Deck D by flowing through the spacecraft, channeled by the solar panel or through the MLI. Additional factors could include an additional leak source near PITMS or channeling of oxidizer from the leak by other spacecraft components to PITMS. Further modeling of this phenomenon to inform future missions is currently being conducted.

Simulations indicate that the leak may have resulted in a temporarily collisional gas environment that increased mass transfer to PITMS, creating a high enough pressure outside the dust cover to equilibrate with the mass analyzer cavity. The continued detection of oxidizer by PITMS days after the first occurrence of the leak implies that this path continued to be active throughout the mission, even as the apparent magnitude of the leak dissipated according to Astrobotic press releases. If the cloud outside PITMS dissipated after an initial burst of pressure, the oxidizer would have to have stayed trapped within PITMS for tens of hours between the anomaly and the first data collection. This would only be possible if NO and NO_2 have long adsorption lifetimes on the internal surfaces of PITMS, but experiments exposing the GRM aluminum surfaces to NO_2 did not confirm sufficiently long lifetimes against pumping action at room temperature. The hygroscopic white paint on the inside of the dust cover might also have adsorbed oxidizer during a period of high external abundance. This surface was part of the internal volume of PITMS while the dust cover was closed and then out of the line of sight of the PITMS aperture once the dust cover was opened. However, features consistent with oxidizer were still present once the door had been open for about 20 hr (last data collection, ITL 18). We conclude that a substantial amount of MON-25 (up to 10^{-7} mbar) was most likely present outside PITMS throughout all data collection periods.

[18] Sandia labs: sparta.sandia.gov.

5.2. Sources of Volatiles on CLPS Landers

As demonstrated in previous sections, PITMS was able to observe a variety of gases during flight, where the most likely source of gases is the spacecraft and instruments on board. As discussed in Section 4.7, no obvious terrestrial atmosphere contribution was detected during the time of PITMS operation, indicating successful venting of atmospheric species with the dust cover closed within the first 34 hr of the mission (prior to PITMS turning on). Atmospheric constituents (N_2, O_2, Ar) do not significantly stick to the spacecraft surfaces and thus fully evacuate orders of magnitude more rapidly than water.

PITMS itself was designed for low outgassing, with the exception of the white paint on the inside of the dust cover, which was intended to reduce solar absorption once the dust cover was opened. PITMS, along with all the other instruments and the Peregrine lander itself, was exposed to the terrestrial atmosphere long enough for the hygroscopic white paint to become saturated with atmospheric water prior to launch. No spacecraft-level bakeout was performed, and although PITMS had the capability built in to perform its own bakeout, the team was not able to perform this operation in flight. The first several spectra have a very clear abundance of water that may be attributed to the first use of the filament and the resulting heating and outgassing effects, but evidence of water persists throughout the mission.

Using the dimensions of the PITMS dust cover and assuming adsorption five molecules deep over the full available surface yields an estimate of about 1.3×10^{17} molecules, or 4 μg, of absorbed water at launch. Prior to opening the dust cover, the PITMS evacuation speed is estimated at about 12 l s^{-1}, which at a pressure of 1×10^{-5} mbar (the pressures PITMS observed with its dust cover closed; Table 3) is about 2×10^{15} molecules s^{-1} escaping to space. This rate would have expended all the door-adsorbed water in less than 24 hr after leaving the atmosphere. What is surprising is the lack of a major rise in water pressure each time we activated the filament and warmed the interior of PITMS. A possible explanation for the lack of a significant rise in water is that solar energy served as a passive instrument bakeout. During the recovery from the propulsion anomaly and prior to PITMS operations, Deck B reached a temperature of 46°C (Figure 3). The warmest PITMS reached during data collection, based on its internal thermocouple, was 44°C; therefore, if Deck B is a good proxy for PITMS temperature, PITMS had effectively already been baked for several hours at slightly warmer temperatures than the warmest operations, releasing sufficient water as to make the change in temperature during PITMS operations too small to create a measurable signal.

Therefore, we conclude that the most likely source for the water, particularly with the dust cover open, is offgassing from the spacecraft. B. Schläppi et al. (2010) note that the dominant source of spacecraft outgassing during the first 200 days of the

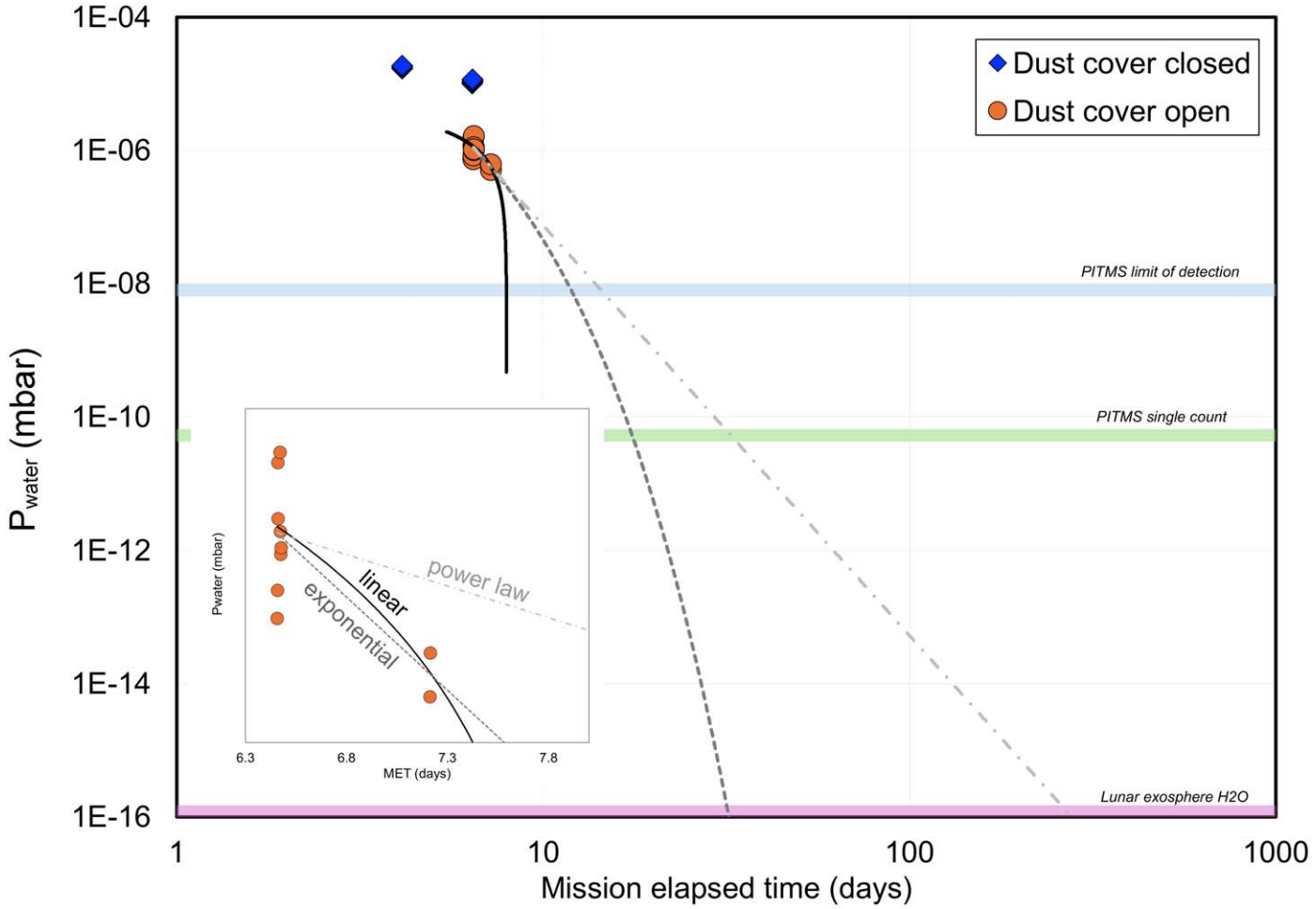

Figure 12. Estimated time required for water to dissipate from the Peregrine lander in space to the limits observable by PITMS. Linear, exponential, and power-law fits to the PITMS data after the dust cover was opened are shown in the inset on a linear scale and in the main panel on a logarithmic scale. Note that the PITMS data are sparse and do not provide very meaningful constraints to the fit (all fits have relatively low R^2 values).

Table 9
Estimated Time for Peregrine Outgassing Water to Dissipate to the PITMS Detection Limits and to the Lunar Exospheric Background

Threshold	Partial Pressure (mbar)	Time to Reach Threshold (Earth days)		
		Linear $y = -7.59\text{E-}7x + 6.03\text{E-}6$	**Exponential** $y = 3.68\text{E-}4\ e^{-9.00\text{E}-1\,x}$	**Power law** $y = 1.05\text{E-}1\ x^{-6.15}$
AB-1 PITMS LOD	8.00×10^{-9}	8	12	14
AB-1 PITMS single count	5.30×10^{-11}	8	18	32
Lunar exosphere water	1.20×10^{-16}	8	32	269

Rosetta mission was desorption of water from exposed surfaces, estimating a half-life of ~21 days for the decay of water density around a spacecraft at 1 au. Here we estimate the water abundance and decay time for the Peregrine spacecraft, assuming that the water measured by PITMS with its dust cover open was solely due to offgassing from the Peregrine spacecraft (and not internal to PITMS).

Following dust cover deployment 154.47 hr into the mission, the partial pressure of water inside the mass spectrometer (sum of OH^+, H_2O^+, and H_3O^+) dropped immediately to $\sim 8 \times 10^{-7}$ mbar and continued to decrease for the remainder of the mission (Table 7). We fit the PITMS observations with linear and exponential extrapolations (Figure 12) to calculate how long it would take until the water pressure reached the PITMS LOD, the single count value (Section 3.2), and the native lunar exosphere (W. M. Farrell et al. 2023). The half-life of the exponential decay rate is 18.5 hr and implies that the outgassing would reach the PITMS detection limit in 12 days and the lunar exospheric background in about a month (Table 9). These calculations represent the offgassing time in space, or an upper limit to outgassing times on the Moon, because the temperatures on the lunar surface would be expected to warm the lander, substantially accelerating the offgassing time.

5.3. PITMS Sensitivity and Potential for Exospheric Detection

As described in Section 3.2, PITMS underwent preflight laboratory calibration analysis that compared the PITMS spectral count values to the partial pressures from an industrial-grade RGA and calibrated pressure gauge. One

Table 10
Lunar Exospheric Species Partial Pressure and PITMS Detection Thresholds[a]

Species	n (cm^{-3})	T (K)	P (mbar)
Starship water outgassing	$>10^{9}$[b]	300	$>4.2 \times 10^{-8}$
PITMS LOD, single spectrum	2×10^{8}	300	8×10^{-9}
Starship water deposit	$>10^{7}$	150 (polar surface)	$>2.1 \times 10^{-10}$
PITMS single count value	1×10^{6}	300	$5.3 \times 10_{-11}$
^{40}Ar	8×10^{4}	300	3.4×10^{-12}
He	3×10^{4}	130 (night)	5.4×10^{-13}
H_2	3×10^{3}[c]	300	1.3×10^{-13}
Ne	3×10^{3}	300	1.3×10^{-13}
^{36}Ar	3×10^{3}	200 (dusk)	8.6×10^{-12}
CH_4	450	200 (dawn)	1.3×10^{-14}
Na	500[d]	300	2.1×10^{-14}
K	40[d]	300	1.7×10^{-15}
O	>11[e]	300	$>4.6 \times 10^{-16}$
H_2O	<3[f]	300	1.2×10^{-16}

Notes.
[a] References providing source information for each natural species are listed in Table 1 of W. M. Farrell et al. (2024).
[b] Assuming a Space Shuttle–like outgassing rate and PITMS within 50 m of the lander.
[c] H_2 density estimates range from ~1.2 to 9×10^3 cm^{-3} (D. M. Hurley et al. 2017). The value used in the table represents the log average of the two range endpoints.
[d] The exospheric density is converted from the column densities shown in Table 1 of W. M. Farrell et al. (2024) assuming a scale height of 100 km (10^7 cm). Column densities originally from A. Colaprete et al. (2016).
[e] The quoted O density is the energic atomic oxygen component and represents a lower density limit.
[f] Exospheric water density lower limit from R. R. Hodges & W. M. Farrell (2022).

PITMS count at $m/z = 28$ was consistent with a N_2 partial pressure of 5.29×10^{-11} mbar (±33%). It is assumed that the sensitivity thresholds at the other mass channels are similar to that at an m/z of 28. Given that the noise fluctuations in the mid-m/z range channels are about ±50 counts, the instantaneous noise fluctuation level is approximately $N \sim 3 \times 10^{-9}$ mbar. For a detection threshold having an S/N of 3, a measurable signal would need to be $\sim 8 \times 10^{-9}$ mbar.

As shown in Section 3.4, integration of PITMS spectra on the lunar surface could have reduced random noise to allow a weaker but persistent signal to be detected. For example, if 1000 measurements were to be averaged, then the random noise fluctuation level would drop by a factor of ~30 to 9×10^{-11} mbar. For an S/N of 3, a detectable threshold would then have been near 3×10^{-10} mbar. Though we did not acquire this many spectra during the as-flown mission, during a nominal surface mission, this number of spectra would encompass approximately 11 hr of nominal PITMS operation, well within the scope of planned operations.

We can compare these PITMS sensitivities to species of the natural lunar exosphere (W. M. Farrell et al. 2023). Given a species number density n and gas temperature T, the gas pressure can be derived using the formula $P \sim 10^4\, n\, k\, T$, where P is in units of mbar, n is in units of cm^{-3}, k is Boltzmann's constant, and T is in units of K. We note that for collisionless exospheric species at the Moon, the effective temperature of the surface-released atoms is directly related to the surface temperature at the emission location, $T \sim T_s$ (e.g., M. Benna et al. 2015). In a surface-bounded exosphere, the pressure on a surface from the gas results from atoms that are "hopping" from one location to another in a series of adsorption/desorption steps. Thus, the pressure is an effective momentum flux of the collisionless atoms onto any exposed surface, including the PITMS opening. Table 10 lists the momentum flux (pressure) for some of the dominant exospheric species in the lunar exosphere.

As shown in Table 10, ^{40}Ar is considered the densest natural species in the exosphere, having a density value close 10^5 cm^{-3}. For ^{40}Ar dayside surface desorption from a surface at 300 K (R. R. Hodges & P. R. Mahaffy 2016), the momentum flux (pressure) of the "jumping" atoms onto the surface is $\sim 3.4 \times 10^{-12}$ mbar. This natural ^{40}Ar partial pressure is about a factor of 10 below the PITMS single count level in the configuration flown on the Peregrine Mission-1.

However, the PITMS ionizing emission current was set to a relatively low value (PITMS was only operated at 20 μA compared to a maximum permissible value of 100 μA) and could have been increased by at least a factor of 5, leading to a corresponding factor of 5 improvement in sensitivity. Additional improvements in future versions of the EMS (see Section 6) are expected to increase the instrument detection threshold by a factor of ~20 or more, enabling a detection of ^{40}Ar at the lunar surface. ^{40}Ar is present in the exosphere throughout the lunar dayside (M. Benna et al. 2015), and there would be many days to weeks available for spectral integration of this gas for a future landed mass spectrometer.

The upper limit of abundance of water in the natural lunar exosphere (outside of meteor shower events) is currently set by the detection threshold of the extremely sensitive neutral mass spectrometer on board LADEE (P. R. Mahaffy et al. 2015; M. Benna et al. 2019a). This upper limit of <3 cm^{-3} (R. R. Hodges & W. M. Farrell 2022), during dayside thermal desorption from a surface at 300 K, would produce a natural water momentum flux (pressure) for the hopping molecules of $<1.2 \times 10^{-16}$ mbar. This partial pressure at $m/z \sim 18$ would have been below the PITMS sensitivity level, and indeed, a challenging measurement for any future in situ mass spectrometers to make.

While the natural water exosphere would not be easily detected by PITMS, the water exosphere created by human systems would be readily observable, making PITMS an ideal sensor to derive the anthropogenic water outgassed from the landing vehicle. Predicted anthropogenic water levels are shown at the top of Table 10. Specifically, the surface area of the Starship lander (~1400 m^2) is comparable to that of the Space Shuttle (~1900 m^2). Also, both bodies will have been exposed for many days to the natural terrestrial weather and humidity at their launch site. W. R. Paterson & L. A. Frank (1989) found that the measured water ions from the Space Shuttle were formed by a co-orbiting neutral water outgassing cloud having a gas density $>10^9$ cm^{-3} within 50 m of the Shuttle. This volatile outgassing was passive, being associated with diffusion and desorption from the spacecraft body. This continuous outgassing was not part of planned thruster or water dump sequences. Over an 8 day Shuttle mission, this passive outgassing was calculated to add about 500 kg of water to the local environment.

Because of their comparable surface areas and long-term exposure to terrestrial gases, we would expect Starship to outgas at a similar rate as the Shuttle. However, Starship is not

expected to return to Earth, so it should eventually be cleaner than the Shuttle was. As listed in Table 10, for a water density of $>10^9$ cm^{-3} at locations within 50 m of the spacecraft and a spacecraft outer surface temperature of 300 K on the sunlit side, the Starship outgassing water partial pressure would be exceed 4×10^{-8} mbar in regions of tens of meters to the spacecraft. Such a pressure would have been readily detectable with PITMS at >750 counts at an m/z of 18.

PITMS may also have been able to detect the water desorbed over time from the volatile deposit created during the Starship landing. W. M. Farrell et al. (2024) found that the Starship propulsion plume could create an extended surface volatile deposit containing ∼70–80 T of water. As shown in their exosphere analysis, for a period of 1 lunar day after the landing, about 1% of this water mass (∼750 kg) resides in the local exosphere, corresponding to an average water exosphere density in half-sphere of 100 km volume of approximately 10^7 cm^{-3}. However, this density is expected to be ∼10 times higher for locations in the near vicinity of the deposit (e.g.,, P. Prem et al. 2020). Such exospheric water density levels originating from the deposit should be detectable by PITMS with a few to ∼100 counts.

We thus find that small, lightweight mass spectrometers like PITMS would be desirable on future Starship landings to monitor the anthropogenic water outgassed from Starship and its plume deposit as a function of time. Such an instrument would be responsive to the high-priority Artemis III Science Definition Team goals of assessing and understanding "the impact human exploration has on the volatile record across the surface" (R. C. Weber et al. 2020).

6. Conclusions

PITMS was one of the first instruments to be built and flown in the CLPS paradigm. PITMS was built and delivered with a small budget and tight schedule, with few requirements other than to "do no harm" to the lander and other instruments. The mission itself did not land on the lunar surface as intended and operated in a spacecraft emergency mode for the entirety of the mission. Therefore, the instrument capabilities were limited, and many aspects of the premission planning were not able to be implemented (detailed in B. A. Cohen et al. 2024). Nonetheless, many lessons learned from the PITMS investigation may be applicable to other teams providing instruments for upcoming CLPS missions or other low-cost, high-risk endeavors.

The ability for any mass spectrometer to meet detailed science objectives, such as measuring the isotope signatures of water and other volatiles to infer their origin and determining the composition of trace compounds as potential contaminants for future water-ice extraction, will depend not only on the innate sensitivity and operation of the instrument itself but also on characterizing and minimizing the contribution of spacecraft outgassing by placement on the spacecraft, the cleanliness of the spacecraft and the instrument, and bakeout procedures before the measurements. PITMS observed persistent water offgassed by the spacecraft. PITMS data show that the spacecraft was outgassing $\sim 1 \times 10^6$ mbar of water a few days into its cruise phase, with a decay half-life of ∼18 hr (though the half-life is only weakly bounded by the sparse PITMS data). This represents substantially more water with a much shorter half-life than the degassing background measured on the Rosetta and Solar and Heliospheric Observatory spacecraft (B. Schläppi et al. 2010), implying that release of a much larger water load was the major source of water detected by PITMS. Landing on the lunar surface would have increased the temperature of the lander and instruments, which would have accelerated offgassing rates. Though PITMS could calculate its own offgassing rates from our materials list, we did not have the same insight into the spacecraft or other payloads, so the amount of water we calculated represents the sum for the lander itself plus all the other payloads, which may or may not have applied their own cleanliness procedures. Offgassing water is not just an issue for mass spectrometers; water can condense onto optical surfaces, degrading such instruments (anecdotally, offgassing water iced the NIRVSS detector in flight). Future CLPS landers may wish to consider the scientific aims of the instruments being delivered and take steps to maintain lander cleanliness and mitigate spacecraft offgassing.

PITMS successfully detected the known oxidizer leak caused by the propulsion system anomaly, and our measurements constrain the nature of the anomaly. First, the leak must have released oxidizer quickly enough to cause total dissociation of N_2O_4 into NO_2 due to a nearly instantaneous pressure drop. Second, the leak may have developed underneath the MLI rather than jetting out directly to free space, because the high abundances of oxidizer seen by PITMS on the opposite side of the lander imply that the oxidizer traveled within the lander surfaces to reach PITMS. The convoluted path of the leak may have contributed to a complex perturbation to the spacecraft attitude. PITMS also detected uncombusted fuel and possibly traces of combustion of the fuel and oxidizer that may help constrain when and how well they were in contact with each other. The ability to detect unreacted oxidizer and fuel as a result of incomplete combustion during lander descent or postlanding venting of propellant would further diagnose the efficacy of spacecraft propellant systems as well as their potential impact upon the lunar environment. The PITMS results show the serendipitous value a mass spectrometer brought to the test flight of a new spacecraft, providing chemical environment data to enhance the context provided by temperature sensors, cameras, and other instruments.

The EMS used on PITMS provided ESA with a prototype and hands-on experience that will benefit future iterations of EMS in the PROSPECT and LUPEX missions. These models will have several improvements over PITMS, including (a) increased sensitivity through running at a higher electron emission current and further optimization of the electron gate and lens design (estimated at an order-of-magnitude improvement in sensitivity), (b) improved detection limits through reducing the background signal by removing polymeric materials from the ITMS chamber to reduce outgassing rates (estimated at an order-of-magnitude improvement in detection limit) and by varying electron gate and lens voltages to help reduce detection of untrapped ions formed natively at filaments during the ring electrode voltage ramp; and (c) incorporation of an onboard calibration gas system to enable in-mission calibration of both the m/z scale and the quantitative response of the mass spectrometer.

Though PITMS was not successful in measuring the native lunar exosphere, we have demonstrated in this paper the capabilities of a mass spectrometer on board a lunar lander, along with lessons in pragmatism and flexibility that would enable such an instrument to ultimately be successful in the CLPS program. Landed mass spectrometers are uniquely

positioned to assess the volatile components of the lunar regolith and exosphere and observe their behavior from dawn to dusk, addressing NASA science and exploration goals. Though manifested individually, multiple mass spectrometers going to the lunar surface should be thought of as a cohesive network that will provide temporally and spatially resolved measurements of exospheric species of interest to both science and human exploration, particularly from multiple landing sites and during different seasons. We recommend that NASA continue to invest in mass spectrometry instrumentation and deploy these capabilities as frequently as possible, ideally in more numerous and more capable situations (longer lifetimes, terminator/overnight operations, etc.). A coordinated campaign of exospheric mass spectrometry measurements, linking observations made from global locations, through diurnal and seasonal cycles, and under other effects like meteor showers and robotic and human activities, will help resolve high-priority, decadal-level science questions and enable informed decision-making about lunar resource availability and utilization.

Data Availability

PITMS data (Deck D thermocouple data, raw data, calibrated spectra, and peak areas) are archived in the PDS (B. A. Cohen & O. J. Tucker 2024).

Acknowledgments

PITMS was developed under the NASA Provided Lunar Payloads (NPLP) program, and EMS was developed as a Moon Mission of Opportunity within the SciSpacE program of ESA's Human and Robotic Exploration program. PITMS was manifested using the Commercial Lunar Payload Services (CLPS) initiative. We are deeply grateful to the NASA and Astrobotic payload managers, engineers, and others who helped ensure PITMS had a successful mission on board Peregrine, including Ryan Stephan, Paul Niles, Jocelyn Mackay, Michael Chahin, Hailey Moosbrugger, Jodi Coletti, and Ander Solorzano. We thank the PITMS instrument development team, our partner institutions, all the other payloads who shared planning and operations with us, and CLPS and Astrobotic for a wild ride.

PITMS work was supported by NASA under the NASA Provided Lunar Payloads (NPLP) program and via award number 80GSFC21M0002 to CRESST for A.J.G. M.J.P. thanks the SEAL team for supporting his participation on PITMS. P.P. acknowledges additional support from NASA through the SSERVI LEADER team (80NSSC20M0020). S.B. was supported by the NASA Postdoctoral Program (NPP). EMS is a program of and was funded by ESA and was developed by The Open University supported by UKRI STFC RAL Space. We thank ESA and the PROSPECT team for supporting the PITMS international investigators.

ORCID iDs

Barbara A. Cohen https://orcid.org/0000-0001-5896-5903
David J. Heather https://orcid.org/0000-0001-7338-0225
Andrew D. Morse https://orcid.org/0000-0001-9683-316X
Michael J. Poston https://orcid.org/0000-0001-5113-1017
Parvathy Prem https://orcid.org/0000-0001-8369-8587
Roland Trautner https://orcid.org/0000-0002-5190-2894

References

Andrews, D. J., Morse, A. D., Barber, S. J., et al. 2012, P&SS, 66, 179
Astrobotic 2019, Peregrine Lunar Lander, Payload User's Guide, https://www.astrobotic.com/wp-content/uploads/2021/01/Peregrine-Payload-Users-Guide.pdf
Astrobotic 2024, Peregrine: Mission 1, Post-Mission Report August 2024, https://www.astrobotic.com/wp-content/uploads/2024/08/PM1_Post-Mission-Report_2024-1.pdf
Benna, M., Hurley, D. M., Stubbs, T. J., Mahaffy, P. R., & Elphic, R. C. 2019a, NatGe, 12, 333
Benna, M., Mahaffy, P. R., Halekas, J. S., Elphic, R. C., & Delory, G. T. 2015, GeoRL, 42, 3723
Benna, M., Malespin, C. A., Hurley, D. H., et al. 2019b, LPSC, 50, 2364
Brady, B. B., & Syage, J. A. 1995, Dissociative Ionization of Methylated Hydrazines, Aerospace Report TR-94(4231)-7, Mechanics and Materials Technology Center https://apps.dtic.mil/sti/tr/pdf/ADA294733.pdf
Cohen, B. A., Barber, S. J., Driggers, P. A., et al. 2024, PSJ, 5, 212
Cohen, B. A., & Tucker, O. J. 2024, NASA Planetary Data System urn:nasa:pds:clps_to_2ab_pll.pitms::1.0, NASA
Colaprete, A., Sarantos, M., Wooden, D. H., et al. 2016, Sci, 351, 249
Donaldson Hanna, K. L., Benavente, J., Bennett, K., et al. 2023, LPSC, 54, 2152
Farrell, W. M., Halekas, J. S., Horányi, M., et al. 2023, RvMG, 89, 563
Farrell, W. M., Prem, P., Hurley, D. M., Tucker, O. J., & Killen, R. M. 2024, PSJ, 5, 105
Harvey, B. 2023, Future, Japan in Space: Past, Present and Future (Berlin: Springer), 345
Hodges, R. R., & Farrell, W. M. 2022, GeoRL, 49, e2022GL099351
Hodges, R. R., Jr., & Mahaffy, P. R. 2016, GeoRL, 43, 22
Hoffman, J. H. 1975, NASA Technical Report NASA-CR-150946, NASA
Hou, L., Fu, P., & Ba, Y. 2019, CST, 191, 2208
Hurley, D. M., Cook, J. C., Retherford, K. D., et al. 2017, Icar, 283, 31
Lee, K. H. 2017, PLoSO, 12, e0176423
Lee, K. H. 2019, AeST, 93, 104882
Leenson, I. A. 2000, JChEd, 77, 1652
Mahaffy, P. R., Richard Hodges, R., Benna, M., et al. 2015, The Neutral Mass Spectrometer on the Lunar Atmosphere and Dust Environment Explorer Mission, in The Lunar Atmosphere and Dust Environment Explorer Mission (LADEE), ed. R. C. Elphic & C. T. Russell, 27 (Berlin: Springer),
March, R. E. 1997, JMSp, 32, 351
Morse, A., Mousis, O., Sheridan, S., et al. 2015, A&A, 583, A42
Paterson, W. R., & Frank, L. A. 1989, JGR, 94, 3721
Potter, N. 2023, IEEES, https://spectrum.ieee.org/moon-rover
Prem, P., Hurley, D. M., Goldstein, D. B., & Varghese, P. L. 2020, JGRE, 125, e2020JE006464
Schläppi, B., Altwegg, K., Balsiger, H., et al. 2010, JGRA, 115, A12313
Schmehl, R., & Steelant, J. 2003, Flash-evaporation of Oxidizer Spray During Start-up of an Upper-stage Rocket Engine, in 39th AIAA/ASME/SAE/ASEE Joint Propulsion Conf. and Exhibit (Reston, VA: American Institute of Aeronautics and Astronautics)
Schonfeld, J. 2023, in 2023 IEEE Int. Conf. on Systems, Man, and Cybernetics (SMC) (Piscataway, NJ: IEEE), 863
Stern, S. A. 1999, RvGeo, 37, 453
Teolis, B. D., Niemann, H. B., Waite, J. H., et al. 2015, SSRv, 190, 47
Trautner, R., Barber, S., Leese, M., et al. 2021, in Int. Astronautical Congress 150 https://iafastro.directory/iac/archive/browse/IAC-21/A3/2A/62020/
Trautner, R., Barber, S. J., Fisackerly, R., et al. 2024, FrST, 5, 1331828
Trinh, H. P., Burnside, C., & Williams, H. 2019, in Int. Astronautical Congress (IAC) https://ntrs.nasa.gov/citations/20190033304
United States Committee on Extension to the Standard Atmosphere 1976, U.S. Standard Atmosphere (National Oceanic and Atmospheric Administration), https://ntrs.nasa.gov/api/citations/19770009539/downloads/19770009539.pdf
Weber, R. C., Lawrence, S. J., Cohen, B. A., et al. 2020, Artemis III Science Definition Report NASA/SP-20205009602, NASA https://www.nasa.gov/sites/default/files/atoms/files/artemis-iii-science-definition-report-12042020c.pdf
Wright, A. C. 1977, Nitric Acid/Nitrogen Tetroxide Oxidizers, USAF Propellant Handbooks 207, USAF https://apps.dtic.mil/sti/citations/ADA036741